FACULTY OF SCIENCE AND TECHNOLOGY

MASTER THESIS

Study programme / specialisation:
Industrial economics / Contract administration & Investment and finance

The spring semester, **2022**

~~Open~~ / **Confidential**

Author:
Jan-Arthur Skartland Svendsbøe


(signature author)

Course coordinator:
Sigbjørn Landazuri Tveteraas

Supervisor(s):
Hans Joakim Skadsem (University of Stavanger)
Bjarte Odin Kvamme (Schlumberger)

Thesis title:
Validation of equivalent circulating densities (ECDs) in cloud-based well planning platform DrillPlan for offshore wells in Norway

Credits (ECTS): **30**

Keywords:
- Well control
- Drilling fluid
- Pressure & temperature
- Annular pressure losses
- Equivalent circulating density
- DrillPlan, digital well construction solution

Pages: **90**

+ appendix: **0**

Stavanger, **15.06/2022**
date/year

Abstract

This master thesis is written in collaboration with Schlumberger. Schlumberger wanted a validation study of equivalent circulating density (ECD) modelling for offshore wells in Norway. The accuracy of ECD modelling in their cloud-based digital well construction solution, DrillPlan, was investigated.

ECD is a very essential aspect of well construction that needs to be understood in order to maintain well control and avoid incidents while drilling. If the ECD is higher than expected, it can lead to fracturing of formation, and consecutively drilling fluid losses to the formation. The understanding and ability to predict ECD is important when it comes to assessing the risks associated with drilling a well and determining whether the planned well design is feasible or not.

To increase knowledge about ECD accuracy for Norwegian offshore conditions modelled in DrillPlan, well- and drilling data were entered into DrillPlan so that the well planning platform had the necessary information to run the desired ECD simulations. ECD simulations were performed by DrillPlan's hydraulic analysis, using drilling parameters from planning and actual drilling parameters obtained from field operations. The simulated data set was retrieved from DrillPlan, verified, and further analyzed in Microsoft Excel.

In this validation study, one 13.5-$inch$ section, one 12.25-$inch$ section, two 8.5-$inch$ sections and two 6-$inch$ sections were examined. One of the 8.5-$inch$ section had several complexities, and it was considered as an outlier in the dataset, as it turned out that there were additional uncertainties associated with the result. DrillPlan's ability to accurately model the ECD was varying for the sections mentioned above. When comparing simulated ECD-values using actual parameters from DrillPlan with actual ECD-values measured from the field, the deviation was smallest for the 13.5-$inch$- and 12.25-$inch$ section, with an average section deviation of 0.007 SG and -0.006 SG, respectively. Simulated ECD-values for the 8.5-$inch$- and 6-$inch$ sections showed higher average section deviations of -0.013 SG & -0.098 SG (outlier), and -0.020 SG & -0.037 SG (temperature not calibrated), respectively. In other words, DrillPlan is able to model ECD accurately in the shallower, larger hole sizes, but it is showing a tendency to underestimate ECD in the deeper, slimmer hole sizes.

Acknowledgements

First, I would like to thank Integration Manager, Michelle Hjelleset, for giving me the opportunity to write my master's thesis together with Schlumberger. Thank you so much for getting me in touch with Digital Drilling Lead, Bjarte Odin Kvamme, who became my external Schlumberger supervisor.

Bjarte Odin Kvamme, during this time we have had together, I have learned an incredible amount from you. You have very good technical qualities that have benefited me during my thesis. Anyhow, the quality you have that I value the most, is that you are able to see things from my point of view. Thank you very much for taking on the job as my external supervisor, for your availability, and the conversations we have had together. I hope we can keep in touch in the future.

Associate Professor, Hans Joakim Skadsem, some time ago I had a short collaboration with you at the University of Stavanger. After our collaboration I knew right away that I would ask you to be my university supervisor for my master's thesis, and fortunately you said yes. You have been a fantastic supervisor who has given me valuable- and quick feedback every time I have needed it. Thank you for all the answers and advice you have given me during my thesis writing. Hope to see you again.

Thank you to the employees- and my fellow students at the University of Stavanger for a memorable time. During these five years of study, a lot has been learned and I now feel ready for new challenges in a constantly evolving world.

I also want to thank mom and dad for all the support you have given me through life. Without the two of you, I would never have achieved what I have achieved. I highly appreciate that you have made it easy for me to prioritize school and education.

Finally, I want to thank my cohabitant Astrid and our beloved daughter Sigrid. You are both my biggest motivation, and I am so grateful for having you in my life. Astrid, thank you especially for the effort you have made at home and the patience you have shown through my master's studies.

Table of contents

Abbreviations

BHA - Bottom hole assembly

BOP - Blowout preventer

ECD - Equivalent circulating density

ESD - Equivalent static density

HPHT - High pressure, high temperature

HSE - Health, safety, environment

IMS - Intelligent Mud Solutions

LSYP - Low shear yield point

MWD - Measurement while drilling

N.A. - Not available

OBM - Oil based mud

PV - Plastic viscosity

ROP - Rate of penetration

RPM - Revolutions per minute

SBM - Synthetic based mud

SI units - The international system of units

US units - United States customary units

WBM - Water based mud

YP - Yield point

List of figures

List of tables

List of equations

1. Introduction

The petroleum industry wants to drill and prepare new wells for future production in the safest and most efficient way. Low oil prices in the past have led the operator companies to seek optimized well construction phases and reduced costs. This can help ensure profitability even in times when the market is exposed to low oil prices. Today, new challenging wells and sidetracks from older wells are being drilled along large parts of the Norwegian coast. Many of the simple- and easily accessible reservoirs have been completed and abandoned, but there is a lot of oil and gas left in the ground. Reservoir volumes are now lower than before [1], which means that the well construction costs also must be reduced if the production of hydrocarbon is to remain as profitable as before. The more demanding well trajectories have further led to a major development in the petroleum industry. Different advanced well constructions programs have been developed, various formations and drilling fluid behavior are better understood, and more autonomous technological solutions of drilling equipment are available and upcoming in the market.

Always ensuring well control during drilling operations can be argued to be the most important responsibility for involved operator companies. An important factor regarding well control is to always be able to control the drilling fluid density in relation to the expected pore- and fracturing pressure in the formation. If the drilling fluid density used is lower than the existing pore pressure downhole, undesirable and uncontrolled flow from the formation into the wellbore can occur. The flow from the formation can consist of ground water and/or hydrocarbons, depending on the location and hole depth. Influx into the wellbore can reach the surface through a so-called blowout that can harm rig workers and the surrounding environment. A blowout preventer is used as a barrier to prevent such incidents reaching surface if any unforeseen kick from the formation occurs. On the other hand, if the drilling fluid density exceeds the formation fracturing pressure, the formation may fracture, causing drilling fluid to flow into the formation due to pressure differences. The additional dynamic pressure caused by equivalent circulating density (ECD) can lead to dynamic losses (during drilling fluid circulation), even though the well might be stable at static conditions (without drilling fluid circulation). High well pressures can lead to hydraulic fracturing in the formation. This can cause lost drilling fluid circulation, a poor hole cleaning and in worst case a stuck drill string that might have to be abandoned in the wellbore. Aadnoy and Russ state that unplanned events like stuck pipe and lost circulation are the most costly drilling problems, and that such incidents may take 10-20% of the total time spent on a well [2].

To visualize the effect of lost circulation, one can look back at an incident from 19.05.2010 [3]. Equinor (at that time called Statoil) lost well control of the well 34/10-C-06 AT5 at Gullfaks C, but it was not due to an excessive ECD. An illustration of the well 34/10-C-06 A can be seen in *Figure 1.1*. Statoil experienced lost circulation because their drilling fluid did flow through a hole in their 13 3/8" casing and into the formation. The 13 3/8" casing had inadequate technical integrity. Both well barriers, i.e., the drilling fluid and the casing, were

broken, which later led to influx from the reservoir into the well. Statoil then had a big job ahead, as they had to understand the complex downhole problems and restore the well barriers. The incident led to gas emissions on the platform, weakened well barriers and lost reputation. Additionally, the production was stopped from 20. May until 14. July, almost two months. Statoil calculated for this period a total production loss (i.e., exposed) of 1084 million NOK. Other economic losses was estimated to be 677 million NOK [3]. The above example shows that lost well control can lead to large additional costs for operator companies involved. In addition, this real-life example illustrates why studies related to well control is important.

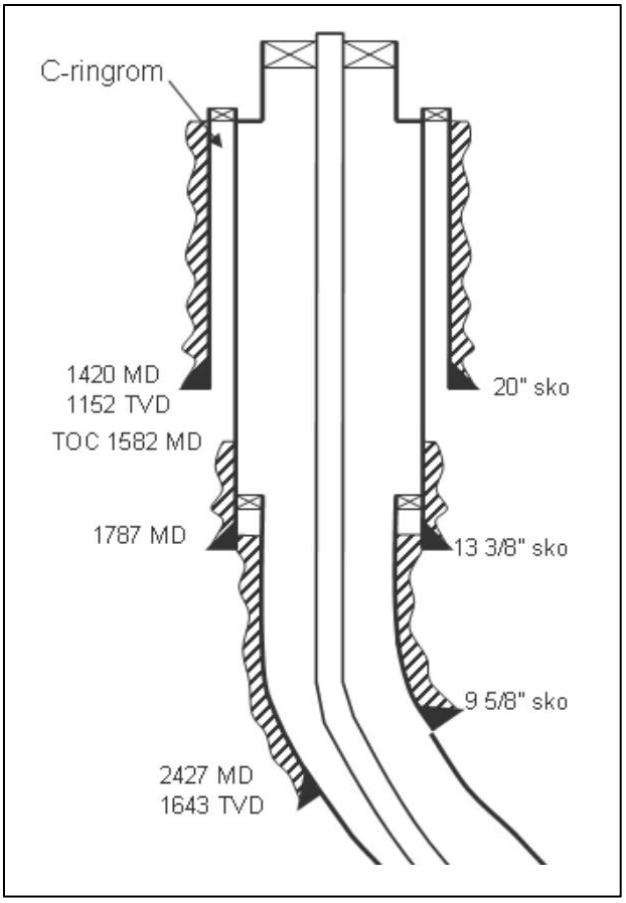

Figure 1.1 - Illustration of the well 34/10-C-06 A.
Statoil experienced lost well control due to a hole in their 13 3/8" casing.
Translation: Ringrom - Annulus & Sko - Shoe.
Source: [3]

Figure 1.2 shows a more generalized example with the rig rental rates on the Norwegian Continental Shelf. Delays and stoppages resulting from lost well control can entail large additional costs only in renting a drilling rig. At the same time all other extra costs such as contracted personnel, supply vessels, hardware and materials etc. associated with the extended drilling time must be covered by the operator company, and by extension the Norwegian Government and people with the current tax regime.

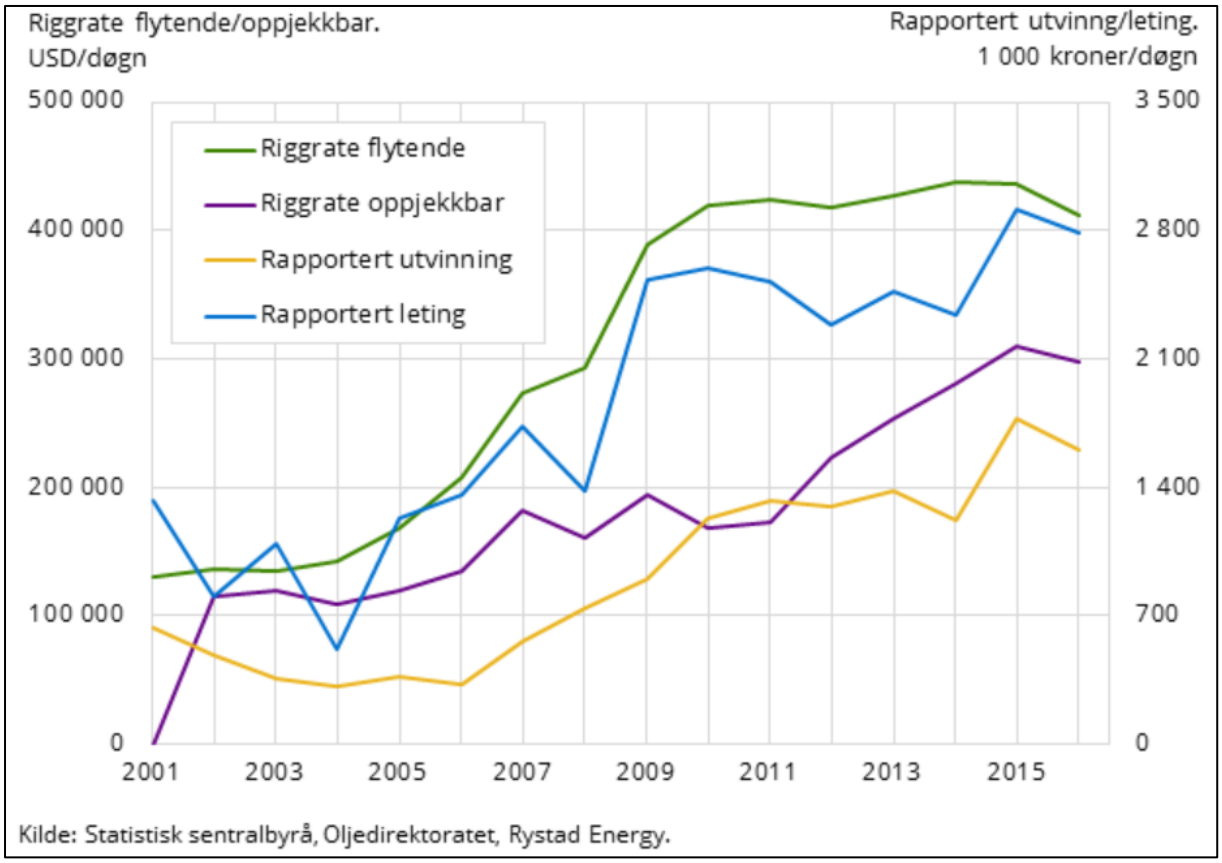

Figure 1.2 - Costs for renting drilling rigs for exploration- and production drilling by rig type in the period 2001 - 2016.
Y-axis to left: Rig rate for semi-submersible and jack-up (USD / day).
Y-axis to right: Reported production and exploration (1 000 NOK / day).
Green - Rig rate semi-submersible. Purple - Rig rate jack-up.
Orange - Reported production. Blue - Reported exploration.
Source:[4]

Blowouts are the worst-case scenarios related to lost well control. A blowout at surface is extremely critical in terms of health, safety and environment (HSE). People, wildlife, nature and equipment can all be severely affected by such an incident. A too high pressure exerted on the formation can also lead to underground blowout, which may be incredibly difficult to take control of. Furthermore, blowouts at surface or underground results in major economical- and reputational costs for the society and the involved companies. Underground blowouts are considered very expensive if a relief well must be drilled to reestablish control of unwanted fluid flows.

1.1 DrillPlan - Cloud-based well planning platform

Schlumberger is developing a well construction planning program called DrillPlan, that aims to provide teams with a common well planning platform, which covers engineering workflows, document preparation and workflow management.

In collaboration with a customer on a high pressure, high temperature (HPHT) well in North Dakota, DrillPlan provided a solution that improved the well planning efficient by more than 50%. In other words, DrillPlan halved the well planning time for the customer and showed its real potential [5]. However, it is important for Schlumberger as an oil service company to fully understand the limitations on their own developed programs. If they succeed in knowing their own limitations, they can manage to deliver services to their customers and meet the customers' expectations. For this reason, Schlumberger wants to investigate how accurately DrillPlan is able to model equivalent circulating density (ECD) for typical wells in the North Sea.

1.2 Objectives

The aim of this thesis is to determine how accurately DrillPlan can model equivalent circulating density (ECD) for typical wells in the North Sea. DrillPlan makes ECD calculations much simpler for a drilling engineer by taking assumptions on many parameters included in the hydraulic model used for ECD calculation. The question is whether these simplifications and assumptions result in accurate results, as the well design can be more complex, and wells are often drilled deeper and longer than typical wells onshore.

To reach these objectives, the following tasks were established:

- Introduce important elements in drilling that are relevant to this study and DrillPlan.
- Explain what ECD is, and why it is an essential part of drilling.
- Perform a literature study of recent work published in the domain of ECD by examining and explaining some of the most important annular pressure drops that may be influencing ECD. Investigate how pressure and temperature generally affect the drilling fluid properties downhole.
- Run simulations and perform a comparison of the calculated ECD values during planning in DrillPlan and the measured values while drilling.
- Prepare a presentation to be held internally in Schlumberger, describing the methodology, comparison results and main findings.

1.3 Structure of the thesis

Theory will be covered in chapter 2, followed by chapter 3, which introduces *Method and implementation*. Simulated results will be presented in chapter 4, *Results*, before they are being discussed in chapter 5, *Discussion*. The uncertainty of the results will be presented in chapter 6, *Uncertainties*, followed by a concluding section, *Conclusion*, in chapter 7. Finally, the bibliography is presented in chapter 8, *References*.

2. Theory

It is very important to be able to control the formation pressure and remove cuttings to maintain well controlling in drilling operations. In the drilling process, drilling fluid helps controlling the wellbore- and formation pressure, as well as contributing to cuttings removal. Additionally, drilling fluids can help by; suspend cuttings, seal permeable formations, minimize reservoir damage, maintain wellbore stability, transmit hydraulic energy to tools and bit, controlling corrosion, ensure adequate formation evaluation, facilitate for cementing and completion, minimize impact on the surrounding environment, lubricate-, cool- and support the bottom hole assembly (BHA) [6].

To avoid uncontrolled well conditions, drilled cuttings must be removed from the wellbore. *Figure 2.1* shows a typical circulating system. Inadequate hole cleaning can lead to cuttings packing together in the wellbore. This is called pack off and in worst case scenarios, pack off can cause drill string to get completely stuck downhole in the wellbore. In these situations, it is possible to cut the drill string, but it results in very expensive equipment being left downhole, if it is not possible to fish the equipment back up to the surface. It is in other words very important to remove the cuttings to maintain controlled hole conditions. A rheological property called viscosity, plays a significant role in hole cleaning. In for example water, which is a low viscosity fluid, cuttings will rapidly settle down, leading to difficulties of circulating out the cuttings. Normally, higher viscosity fluids are used as drilling fluids since they tend to improve cuttings transport with circulation. The cuttings will flow better and not settle as quickly as for a low viscosity fluid. Additionally, drilling fluid viscosity is decisive for pump pressure and consequently equivalent circulating density (ECD).

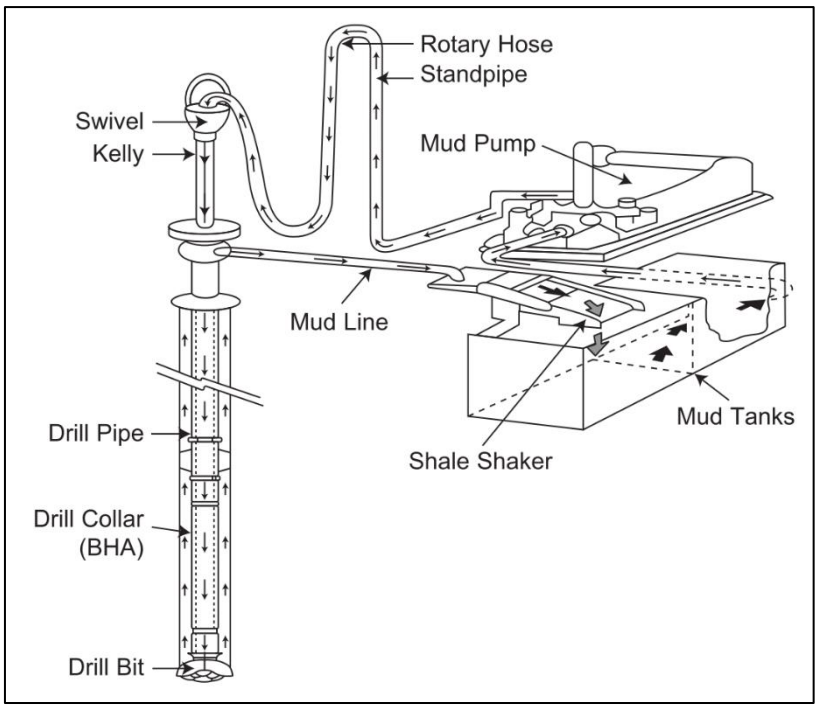

Figure 2.1 - A typical circulating system showing the flow path of the drilling fluid. Source: [7]

For all "normal" drilling situations, always having the right density of drilling fluid is the most important thing. Using a drilling fluid density lower than the formation pressure or pore pressure, may lead to unwanted formation fluids into the wellbore due to pressure differences. The influx of formation fluid will disturb and mix with the drilling fluid, or in worst case result in the need to activate the blowout preventer (BOP) to handle the kick. Too low pressure downhole can also result in cavings and hole collapse, followed by hole cleaning problems. On the other hand, having a too high drilling fluid density, the formation can fracture, leading to losses or total loss of circulation and possible reservoir damage. Due to these consequences, it is vital to always control the drilling fluid density. *Figure 2.2* illustrates simply how the density of the drilling fluid should remain between the pore pressure and fracture pressure window.

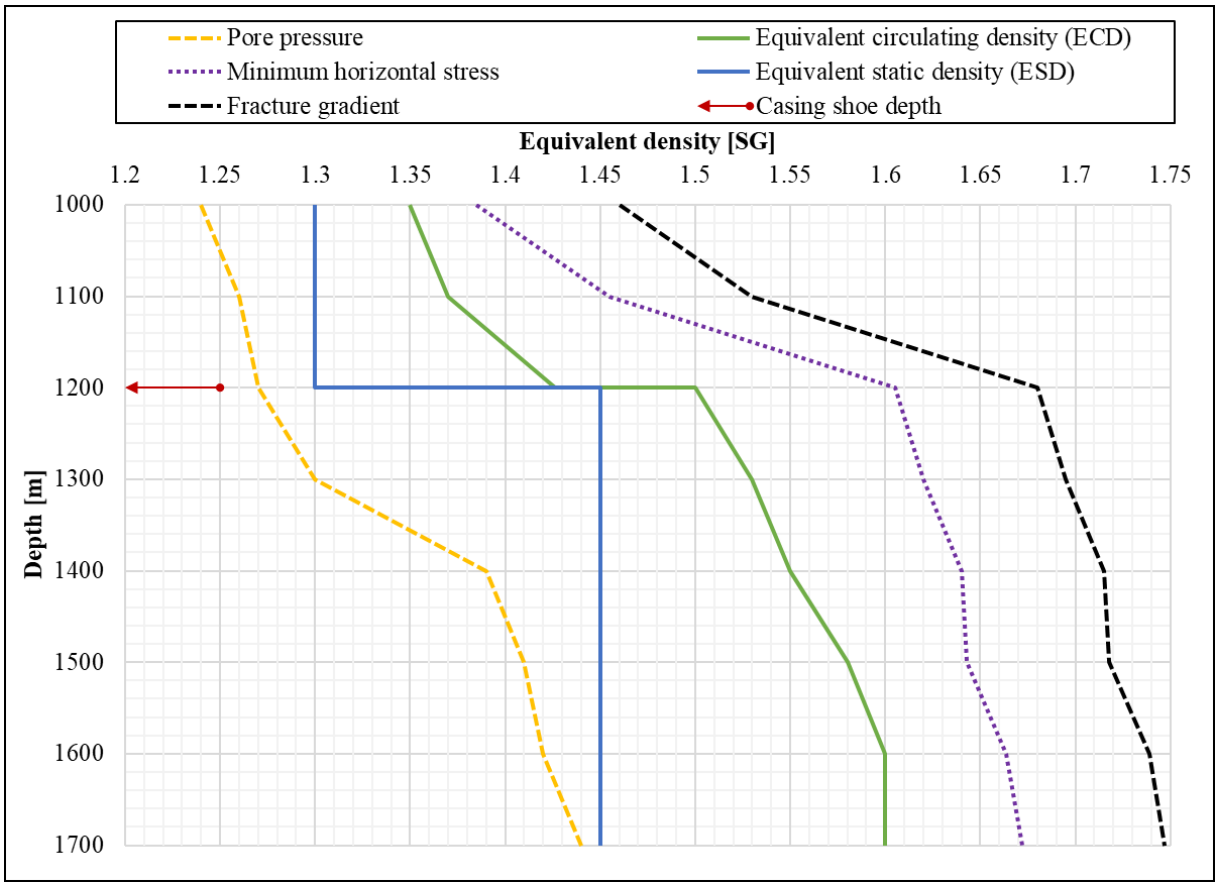

Figure 2.2 – Depth vs. Equivalent density, illustrating drilling fluid density window. Pressure is expressed as equivalent density with SG as unit. In this simplified example, a casing is set at 1200 meter and the drilling fluid density is increased to keep it in between pore pressure and fracture pressure.

2.1 Viscosity

The rheological property of the drilling fluid that indicates its resistance to flow is called viscosity [8]. Viscosity is the ratio of shear stress to shear rate and can be seen mathematically in *Equation 2.1* [9].

Equation 2.1 - Viscosity:

$$\mu = \frac{\tau}{\dot{\gamma}} \qquad 2.1$$

Where (in SI units):

$\mu -$ fluid viscosity $(Pa \cdot s)$

$\tau -$ shear stress (Pa)

$\dot{\gamma} -$ shear rate (s^{-1})

The shearing force over an area exerted on the fluid is called shear stress, τ, while the velocity gradient or fluid velocity/length is the shear rate, $\dot{\gamma}$ [8]. In other words, the force per unit area which is required to sustain fluid flow is the shear stress, and the rate at which the fluid velocity changes with respect to the distance from the wall is the shear rate [9].

It is possible to characterize fluids by their rheological behavior. Newtonian fluids are fluids whose viscosity remains constant with changing shear rate, under otherwise constant conditions. Consequently, non-Newtonian fluids are fluids whose viscosity varies if shear rate changes. Furthermore both the temperature and pressure affect fluids viscosities, and thus it is important to specify the temperature and pressure properly, in order to describe the fluid flow in the best possible way [9].

2.1.1 Newtonian fluids

Newtonian fluids are fluids that have shear stress which is directly proportional to shear rate. Typical examples of fluids that are Newtonian is light oils, brines, water and glycerin. At a given pressure and temperature, a single viscosity measurement characterizes a Newtonian fluid [9].

2.1.2 Non-Newtonian fluids

Unlike Newtonian fluids, non-Newtonian fluids are fluids that have shear stress which is not directly proportional to shear rate. In other words, the viscosity of non-Newtonian fluids varies with shear rate. The vast majority of today's drilling fluids are non-Newtonian [9].

Drilling fluids that exhibit less viscosity at higher shear rates than at lower shear rates are said to be shear-thinning. A pseudoplastic fluid is one type of a shear-thinning fluid that begins to flow as soon as a shear force or pressure, regardless of how slight, is applied. For pseudoplastic fluids, an increasing shear rate causes a progressive decrease in the fluids viscosity. Some shear-thinning fluids are called viscoplastics. These fluids do not flow until a given shear stress is applied, and the shear stress required to get fluid flowing is called the yield stress [9].

There exist some non-Newtonian fluids that exhibit shear-thickening behavior when in laminar flow. The viscosity of shear-thickening fluids increases with increasing shear rate, but this behavior does not often occur in drilling fluids that circulates in a well [9].

Fluids can further be affected by time. Under constant shear rate, the viscosity of a thixotropic fluid changes with time until equilibrium is reached [10]. Gelation or gel-strength development is common for thixotropic fluids. When the fluid remains static for a certain time, there will be an increase in viscosity, and thus, a sufficient force must be exerted on the fluid in order to overcome gel strength to initiate flow. Rheopectic fluids experience an increase in viscosity with time under constant shear rate conditions [9].

The rheological characteristics of drilling fluids are experienced to vary from elastic, gelled solids at one extreme to purely viscous Newtonian fluids at the other. Drilling fluids can exhibit Newtonian, viscoplastic, pseudoplastic, or even other behavior at specific conditions. Due to these facts, it is not very unreasonable to assume that all drilling fluids are viscoelastic. Viscoelastic fluids exhibit both elastic and viscous properties to varying degrees [9].

2.1.3 Methods of measuring viscosity

In the calculation of hydraulics, hole-cleaning efficiency, and prediction of weight material sag in oil wells, it is vital to determine the rheological parameters of the drilling fluid [9]. Funnel viscosity, apparent viscosity, plastic viscosity and effective viscosity are all different terms that describes the drilling fluids at the oil fields [8].

2.1.3.1 Marsh funnel

Marsh funnel, seen in *Figure 2.3,* is a cone-shaped tool with a narrow tube on the bottom end. Due to gravity action, the drilling mud flows through the tool, which results in a simple test for viscosity at the wellsite. This simple test does not provide a true viscosity value, but a relative comparison one. Through measuring a timed rate of flow, one gets a qualitative measurement that indicates how thick the tested drilling mud sample is. The time (in $seconds$) it takes for 1 $quart$ (946 ml) of drilling mud to flow through the Marsh funnel is the viscosity [8]. This measurement is referred to as the funnel viscosity. The Marsh funnel is most useful to alert wellsite personnel to changes in the drilling fluid properties or conditions. Be aware that the funnel viscosity is a one-point measurement, and thus it cannot give any information about why the actual fluid viscosity may be low or high. Furthermore, this method cannot be used to represent a consistent value for all drilling fluids of the same- type or density [9].

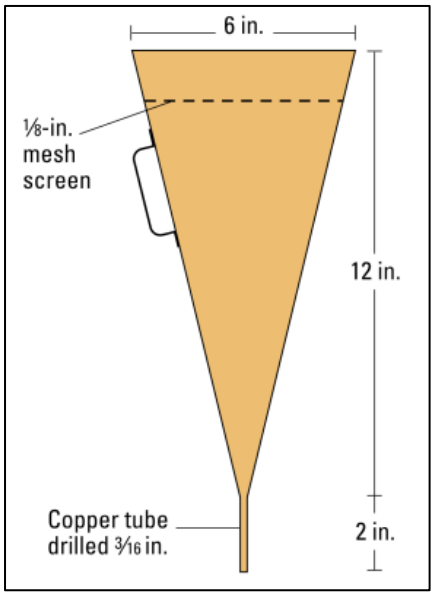

Figure 2.3 – One-point viscosity measurement tool, Marsh funnel.
Source: [11]

2.1.3.2 Rotational viscometer

The tool most used for measuring the rheological properties of drilling fluids, is the rotational coaxial-cylinder viscometer. Couette-type viscometer is another name for the same tool, see *Figure 2.4.* The fluid sample is contained in the annular space between two coaxial cylinders. In the mentioned Couette-type viscometers, the sleeve (outer rotor) is driven at a constant rotational speed, and thereby a torque gets applied on the bob (inner cylinder). A torsion spring that retrains movement, measures the resulting torque on the bob for mechanical Couette viscometers. Attached to the bob there is a dial. It helps indicating deflection of the bob in degrees that is proportional to the shear stress. The same principle and geometry exists for digital viscometers, but here a torque sensor may be used in order to indicate the shear stress [9].

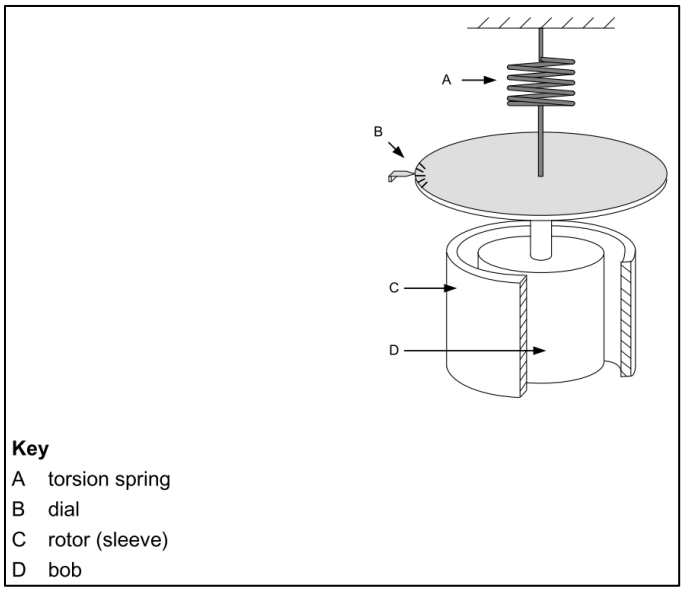

Figure 2.4 – Mechanical rotational viscometer with dial readout – Couette type. Source: [9]

Using a standard spring (F1.0), a standard rotor and a standard bob geometry (known as R1B1), plastic viscosity (PV) and yield point (YP) are directly obtained by readings from rotor speeds of 600 $\frac{rev}{min}$, (R_{600}), and 300 $\frac{rev}{min}$, (R_{300}). Having a rotor inner diameter fixed at 1.450-$inch$ (3.683 cm) and a bob diameter fixed at 1.358-$inch$ (3.449 cm) for R1B1, the ratio (rotor/bob) will be 1.0678, which is a value that meets the international German Institute for Standardization (DIN) standards. Furthermore, dial reading at (R_{300}) is equal to the fluid cP viscosity at a shear rate of 511 s^{-1}, and thus will viscometers of this configuration work as direct reading instruments [9].

Calculation of plastic viscosity and yield point can be seen below, in *Equation 2.2* and *Equation 2.3*, respectively. PV is the part of the flow resistance in a drilling fluid mainly produced by the viscosity of the liquid phase and the friction of the suspended particles [8]. On the other hand, YP is simply the yield stress extrapolated to a shear rate of zero, i.e., where it crosses the y-axis. *Figure 2.5* shows a plot of measured data and a rheological model where these equations are highly relevant.

Equation 2.2 - Plastic viscosity (cP)*:*

$$PV = R_{600} - R_{300} \qquad 2.2$$

Equation 2.3 - Yield point $\left(\frac{lb}{100\ ft^2}\right)$*:*

$$YP = R_{300} - PV \qquad 2.3$$

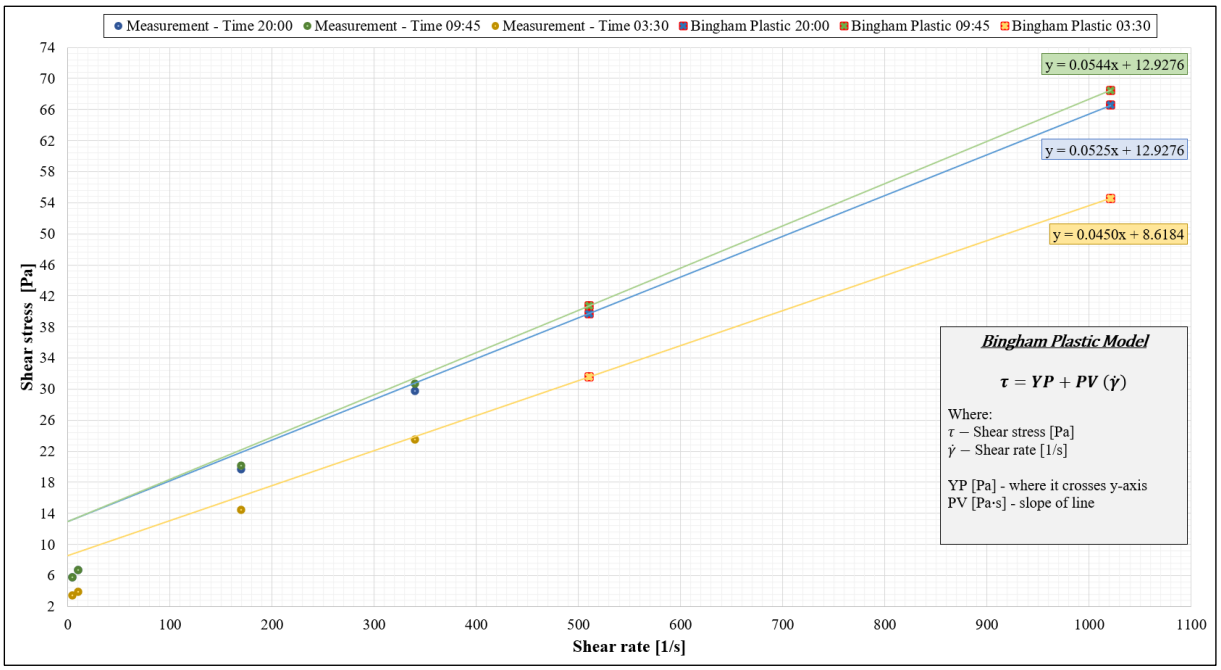

Figure 2.5 - Shear stress vs Shear rate. Measured rheological data can be seen as single points. The dotted lines illustrate the Bingham plastic model associated with these measured data. For these data, it turned out that Bingham Plastic 20:00 and Bingham Plastic 09:45 have equal yield point, but different plastic viscosity. Deviations between Bingham Plastic and measured rheological data can be seen at lower shear rates, i.e., $< 511\ s^{-1}$ (R_{300}).

In addition to provide PV and YP, the rotational viscometer can provide gel strength. The gel strength is (per procedure) measured through the highest dial reading. After stirring the drilling fluid at 600 $\frac{rev}{min}$, initial gel strength is found by keeping the drilling fluid in rest for 10 $seconds$, followed up by viscometer rotation at 3 $\frac{rev}{min}$. At 3 $\frac{rev}{min}$ the initial gel strength can be measured through the highest dial reading. This method is also used for the 10 $minutes$ gel strength, where the only difference is the resting time, which in this case is 10 $minutes$ [8].

2.1.3.3 RheoProfiler 200

M-I SWACO have developed an automated rheometer which provides a thorough, yet straightforward system that is capable of testing rheological properties and densities of all mud types, i.e., water based mud (WBM), oil based mud (OBM) and synthetic based mud (SBM). The RheoProfiler 200 can be seen in *Figure 2.6.* It has a compact design and weighs only 83 lbm (37.6 kg), resulting in a high mobility. The machine has the ability of cooling or heating fluid samples to 40 °F (4.4 °C) or 150 °F (65.6 °C) in less than 10 $minutes$ to perform a range of shear stress tests. For the RheoProfiler 200 to implement its automated tests, a mud engineer must connect the fluid sample to the machine. When the fluid sample is properly attached to the machine, reliable and repeatable method of testing can be guaranteed for any samples. This can result in a higher precision and the repetitive standard measurements tasks for the fluid engineer will be eliminated. Furthermore, the RheoProfiler 200 enables rapid data delivery which will help assist customers with drilling fluid challenges. Measured results will efficiently be sent to stakeholders to improve the well construction performance [12].

Figure 2.6 – M-I SWACO rheometer, RheoProfiler 200.
Source: [13]

2.1.3.4 RheoProfiler 300

RheoProfiler 300 is a fully automated rheometer developed by M-I SWACO which also tests densities and rheological properties of all mud types. The design of the machinery differs from the RheoProfiler 200. Even though the RheoProfiler 300 has a quite compact design with a length of 1.4 m, a width of 0.6 m and a height of 1.5 m, it is much less mobile than RheoProfiler 200, due to its net weight of 340 kg. The RheoProfiler 300 is approved for location in Ex-Zone 1, where the machine directly attaches to the circulation system flowline at the rig site for continuously fluid measurements [14]. In other words, fluid engineers do not need to implement the repetitive task of attaching the fluid samples to the rheometer, like for the RheoProfiler 200. RheoProfiler 300 connected to the circulation system can be seen in *Figure 2.7*. Continuously and rapidly the measured data will be shared. This will assist customers and other stakeholders with drilling fluid challenges and consequently enhance the well construction performance [15].

Figure 2.7 – M-I SWACO rheometer, RheoProfiler 300.
Source: [15]

2.1.3.5 BaraLogix and RheoSense

Halliburton Baroid specializes in drilling fluid. They have developed the BaraLogix to automatically get real-time measures of drilling fluids. Advanced hydraulic software, surface measurement automation and predicative analytics will lead to data-informed decision making [16]. Another company, Intelligent Mud Solutions (IMS) is majority owned by Jektevika AS, NAVIC Group and Equinor Technology Ventures. Their goal is to create a fully automatic real-time analysis of drilling fluid properties [17]. IMS have developed RheoSense which offers autonomous fluid analysis in real time. RheoSense is designed such that it easily can be connected optimally to the fluid process, both in and out of the well [18].

2.1.4 Rheological models

Practical experience combined with knowledge of rheological models is necessary to fully understand the performance of fluids. Rheological models help in fluid flow characterization, but there exists no single model available that completely describes rheological characteristics of drilling fluids over their entire shear rate range. To graphically depict a rheological model, shear stress vs shear rate measurements are plotted in a so-called rheogram. Note that rheological models used for drilling fluids only describe time-independent, purely viscous behavior [9]. *Figure 2.8* illustrates four different rheological models, but due to the degree of relevance in this thesis, only the Herschel-Bulkley model will be further explained in the following subsection.

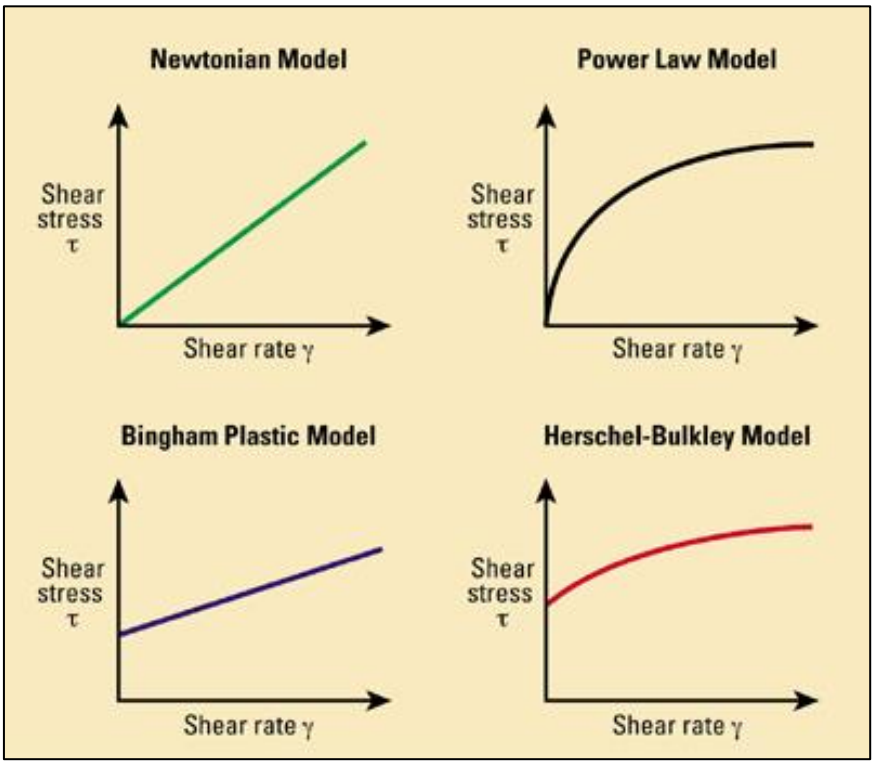

Figure 2.8 – Different rheological models:
Newtonian-, Bingham plastic-, power-law- and Herschel-Bulkley model.
Source: [19]

2.1.4.1 Herschel-Bulkley model

Herschel-Bulkley model is a combined model of the Bingham- and power-law model that regularly provides a very good fit for nearly all synthetic-, oil-, and water based drilling fluids. Sometimes the model is referred to as yield-power-law, modified power law or yield-pseudoplastic model [9]. Herschel-Bulkley model requires three parameters for fluid characterization and the model is defined by *Equation 2.4*, which only is valid for laminar flow [8].

Equation 2.4 - Herschel-Bulkley model:

$$\begin{aligned} \tau &= \tau_y + K\dot{\gamma}^n, \quad && (\tau_y < \tau) \\ \dot{\gamma} &= 0, && (\tau \leq \tau_y) \end{aligned} \tag{2.4}$$

Where (in SI units):

$\tau -$ shear stress (Pa)

$\tau_y -$ yield stress (Pa)

$K -$ consistency index $(Pa \cdot s^n)$

$\dot{\gamma} -$ shear rate (s^{-1})

$n -$ power-law exponent or flow behavior index

Herschel-Bulkley model can represent a Bingham plastic fluid $(n = 1)$, a Newtonian fluid $(n = 1, \tau_y = 0)$, a pseudoplastic fluid $(n < 1, \tau_y = 0)$, a yield-pseudoplastic fluid $(n < 1)$, or a dilatant fluid $(n > 1)$. Yield stress is included from the Bingham model, which entails that the fluid behaves like a solid until the force applied is high enough to overcome the yield stress. On the other hand, the consistency index and power-law exponent are included from the power-law model [8].

Low shear yield point (LSYP) is calculated from viscometer readings R_6 and R_3 and is a common method to approximate the yield stress, τ_y. The calculation of τ_y can be seen in *Equation 2.5*. Another method to find τ_y is to use numerical techniques using weighted- or unweighted parameters. For this purpose, computer programs or spreadsheets are required. It is also possible to use a convergence approach to find the τ_y parameter [9].

Equation 2.5 - Yield stress approximation using low shear yield point:

$$\tau_y \approx LSYP = 2R_3 - R_6 \tag{2.5}$$

The flow behavior index n, and the consistency index K, are calculated using *Equation 2.6* and *Equation 2.7*, respectively [9]. R_{300} can be written as $PV + YP$ from *Equation 2.3*, while R_{600} can be written as $2PV + YP$ from *Equation 2.2*.

Equation 2.6 - Calculation of flow behavior index:

$$n = 3.32\, log_{10}\left(\frac{R_{600} - \tau_y}{R_{300} - \tau_y}\right) = 3.32\, log_{10}\left(\frac{2PV + YP - \tau_y}{PV + YP - \tau_y}\right) \qquad 2.6$$

Equation 2.7 - Calculation of consistency index:

$$K = \frac{\left(R_{300} - \tau_y\right)}{511^n} = \frac{\left(PV + YP - \tau_y\right)}{511^n} \qquad 2.7$$

Be aware that *Equation 2.5*, *Equation* 2.6 and *Equation* 2.7 provides simplified parameter estimates. By using a spreadsheet or similar computational software, it is possible to use all measurement points to best estimate the required parameters. Skadsem et al. used nonlinear regression and all point measurements [20]. Thus, they were able to confirm that the Herschel-Bulkley model provides an accurate fit to drilling fluids. *Figure 2.9* shows that the Herschel-Bulkley model can be a very good model for the two most used drilling fluids; water- and oil-based drilling fluids. The lines are Herschel-Bulkley model fittings for the two different drilling fluids, while the frequent points are rheometer measurements. Dashed line corresponds to the effective viscosity (from the left). Shear stress (to the right) associates to the solid lines [20].

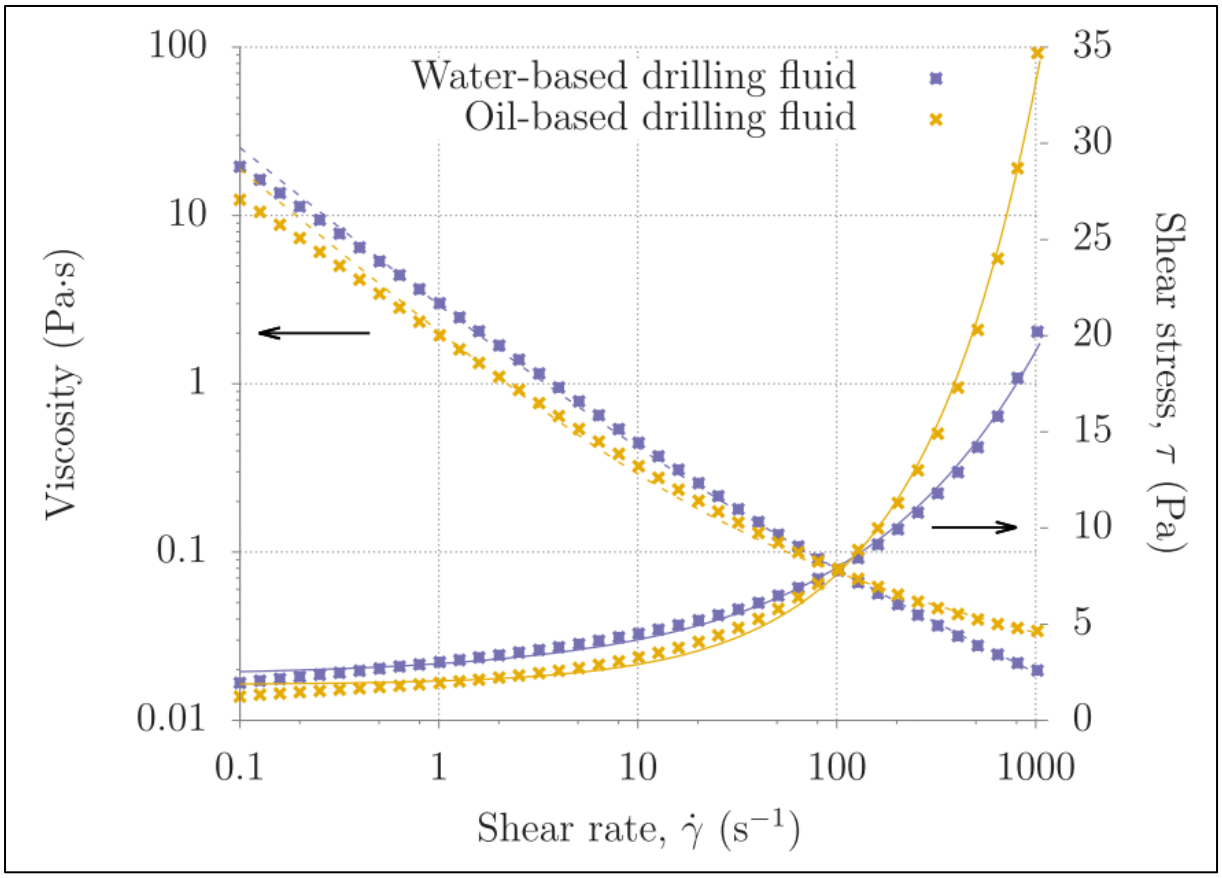

Figure 2.9 - Viscosities and steady state shear stresses for one water based- and one oil based drilling fluid. Points relates to rheometer measurements, dashed line relates to effective viscosity, while solid line refers shear stress.
Source: [20]

The results in *Figure 2.9* illustrates a highly shear thinning water based drilling fluid, meaning low effective viscosity at high shear rates. The estimated Herschel-Bulkley parameters overestimates the shear stress at low shear rates ($< 1\ s^{-1}$). Insufficient measurement time or apparent slip effects may have caused the deviation. Even though the water- and oil based drilling fluids have comparable steady state viscosities, thixotropy measurements and stress overshot indicate different viscosity building [20].

2.1.5 Cuttings transport

Drilled cuttings can effectively be carried in suspension in vertical and near-vertical well sections. Here, the annular fluid velocity helps to overcome the cuttings settling force leading to a net upward movement for the drilled cuttings. In more high-angle well sections, formation of cuttings bed generally occurs on the low side of the hole due to the gravitation force acting on the cuttings. A drag force created by the annular fluid velocity tends to move the cuttings bed along the wellbore. In addition, annular fluid velocity creates a fluid lift force that tends to move the drilled cuttings away from the wellbore and in the direction of the higher velocity flow stream [9]. Drill string rotation may assist moving cuttings up from the cuttings bed into the high velocity flow stream that normally forms the high side of the wellbore.

The flow patterns present in annulus is highly dependent on drilling fluid rheological properties and flow rate. High-viscosity fluids with high- yield point and yield stresses cause cuttings beds to slide, due to increase in the fluid drag force. Less viscous fluids with low-yield points and yield stresses have a tendency to promote cuttings saltation and turbulence [9]. *Figure 2.10* illustrates the transport mechanisms for different- annular velocities and well inclinations, with the assumption of no pipe rotation.

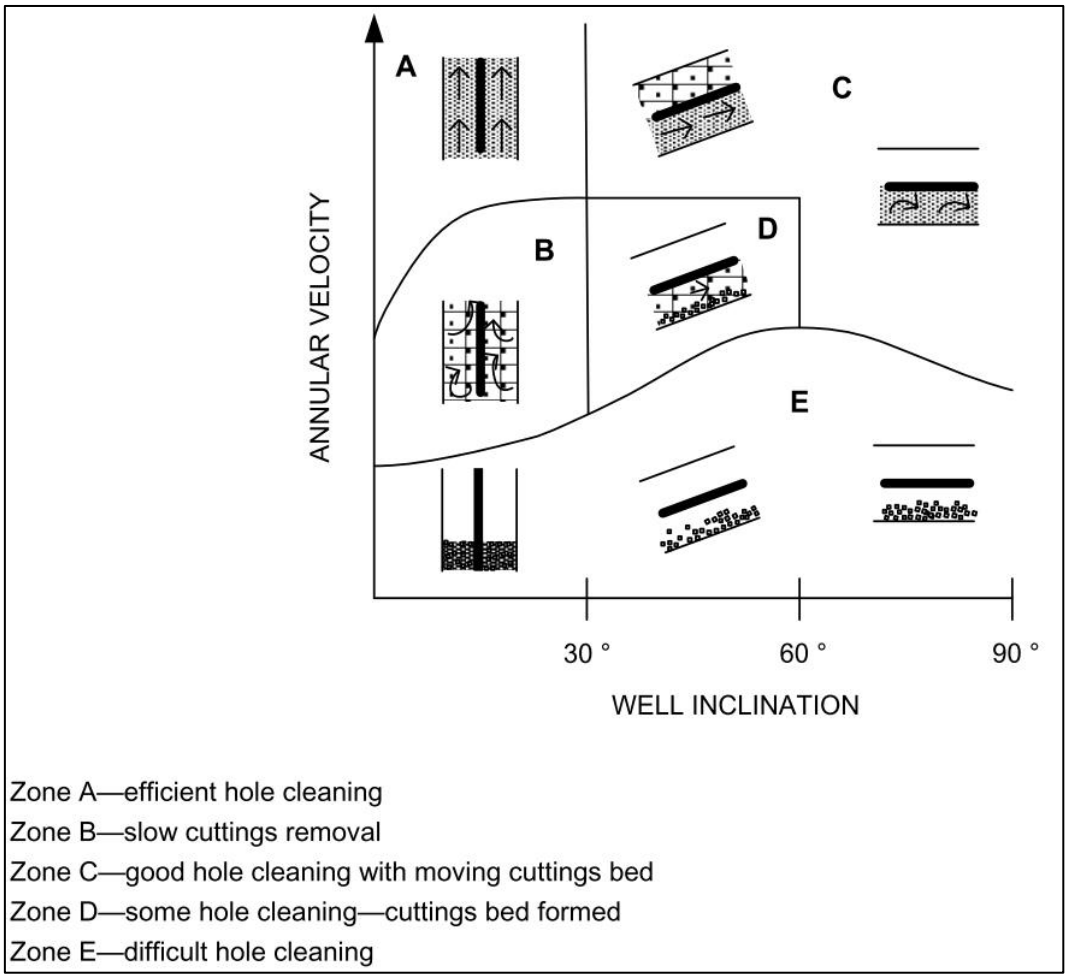

Figure 2.10 - Mechanisms of cuttings transport in near-vertical- and deviated wells. The different zones are separated using the letters A, B, C, D and E.
Source: [9]

Zone- A and B have an inclination lower than 30°. In these zones, beds normally do not form since the drilled cuttings are effectively suspended by the fluid shear, and hence, conventional transport calculations based on vertical slip velocities are applicable. Regarding well inclinations above 30°, drilled cuttings can settle as beds on the low side of the hole. In worst case, the cuttings can slide back down the wellbore and pack-off the annulus. The cuttings at the low side can either be transported as dunes or ripples (as Zone D illustrates), or alternatively as a sliding bed. Anyhow, rotation and reciprocation of the drill string can mechanically obstruct cuttings beds and distribute them in the faster flowing drilling fluid at the high side of the wellbore. Zone E has a high chance of cuttings bed formation and tight-hole problems, while Zone- A and B illustrates the commonly easiest cuttings transport situations [9].

2.2 Density

The definition of density is weight per unit volume and can mathematically be seen in *Equation 2.8* [21].

Equation 2.8 - Density:

$$\rho = \frac{m}{V} \qquad 2.8$$

Where (in SI units):

$\rho -$ density $\left(\frac{kg}{m^3}\right)$

$m -$ mass (kg)

$V -$ volume (m^3)

Density is one of the most important drilling fluid properties. A drilling fluid that has a proper density can control the hydrostatic pressure in a wellbore and prevent unwanted fluid flow from the formation into the well. The density in a drilling fluid also prevents casing- and open hole collapse. Conversely, excessive drilling fluid density can lead to an unwanted lost circulation and the formation can be damaged through fractures [22].

2.2.1 Equivalent circulating- and equivalent static density (ECD and ESD)

The total annular circulating pressure losses from the point of interest to the flow line, plus the hydrostatic pressure of the drilling fluid, is equal to the pressure exerted on a formation while circulating. This combined force is expressed as the density of drilling fluid that would exert a hydrostatic pressure that is equivalent to this pressure, and hence, this equivalent drilling fluid weight is called the equivalent circulating density (ECD). The most common and simplified ECD formula gives ECD in US units and can be calculated using *Equation 2.10* [6]. Using SI units, ECD can be calculated by *Equation 2.9*. To keep it simple, this equation holds the assumptions that density (ρ) is constant and thus independent of pressure and temperature, and that the frictional pressure loss per unit length is constant along the whole depth [23].

Equation 2.9 - Equivalent circulating density (SI units):

$$ECD = \rho + \frac{\left(\frac{\Delta P_f}{\Delta L}\right) \cdot MD}{g \cdot TVD} \qquad 2.9$$

Where (in SI units):

$ECD -$ equivalent circulating density $\left(\frac{kg}{m^3}\right)$

$\rho -$ drilling fluid weight $\left(\frac{kg}{m^3}\right)$

$\left(\frac{\Delta P_f}{\Delta L}\right) -$ frictional pressure loss per unit length $\left(\frac{Pa}{m}\right)$

$MD -$ measured depth (m)

$g -$ gravitational acceleration $\left(\frac{m}{s^2}\right)$

$TVD -$ true vertical depth (m)

Equation 2.10 – Equivalent circulating density (US units):

$$ECD = \rho + \frac{P_a}{0.052(TVD)} \qquad 2.10$$

Where (in US units):

$ECD -$ equivalent circulating density $\left(\frac{lbm}{gal}\right)$

$\rho -$ drilling fluid weight $\left(\frac{lbm}{gal}\right)$

$P_a -$ pressure drop in annulus between bell nipple and TVD (psi)

$TVD -$ true vertical depth (ft)

Equation 2.9 will give a constant ECD for a vertical well since the measured depth will be equal to the vertical depth. For extended reach- and horizontal wells, the ECD which is a function of the ratio of measured- to true vertical depth, will to a great extent increase with the increase of measured depth [23].

ECD represents the well pressure as an equivalent density. This is of interest since drilling fluid and drilling fluid weights constitute the primary barrier in drilling wells. On the other hand, wellbore pressure without circulation is termed equivalent static density (ESD) [8]. ESD is seen as the proper term to determine real downhole hydrostatic pressure [24]. Zamora and Roy clarified that drilling fluid density will vary with pressure and temperature [25]. To get a best ESD estimate as possible, pressure and temperature must therefore be considered when calculating static bottom hole pressure[25].

2.2.1.1 Consequences of too low ESD and too high ECD

Typically drilling hole problems occur when the downhole safe operating pressures limits like pore, collapse and fracture pressure are exceeded. Additional problems can be insufficient hole cleaning, leading to excessive reaming times, packing off and stuck pipe. Pressure limits for well control and wellbore integrity sets the framework for which density window the drilling fluid needs to stay within to avoid pressure boundary exceedances [9].

It is important to always keep ESD above pore pressure to control the formation pressure and avoid unwanted influx into the wellbore. If the pressure from formation is greater than ESD, there is a big risk of getting an uncontrolled blow out as a result from fluid flow into the well. On the other hand, if ECD is greater than the minimum horizontal stress, drilling fluid may be lost to the formation through temporary cracks, leading to stop of fluid circulation in the wellbore. ECD exceeding the fracture gradient will crack the formation permanently. This can lead to drilling fluid losses, no wellbore circulation, unstable downhole conditions, and possible unwanted reservoir damages. A simplified *Figure 2.2*, illustrates how ESD and ECD stays within the density window, which helps avoiding influx from formation and drilling fluid losses. To consider the increasing pore pressure, a casing is set at 1200 $meter$ and the drilling fluid density is increased.

2.2.1.2 Possible flow rate and rate of penetration effects on ECD

ECD can be greatly affected by flow rate. If the flow rate is too low while circulating drilled cuttings, it can result in poor cuttings transport. Cuttings can accumulate in the annulus and consequently increase ECD. Examples of this is illustrated in *Figure 2.11* and *Figure 2.12*, where a flow rate of 1000 $\left(\frac{L}{min}\right)$ clearly results in accumulation of drilled cuttings and a considerable higher ECD, which will be difficult to control. Squared points illustrates ECD with cuttings, while circle points show ECD without cuttings. The effect is greatest in *Figure 2.12*, since the rate of penetration (ROP) is a lot higher compared to the ROP in *Figure 2.11*. Higher ROP results in more drilled cuttings i.e., higher cuttings load, followed by additional cuttings accumulation in the annulus.

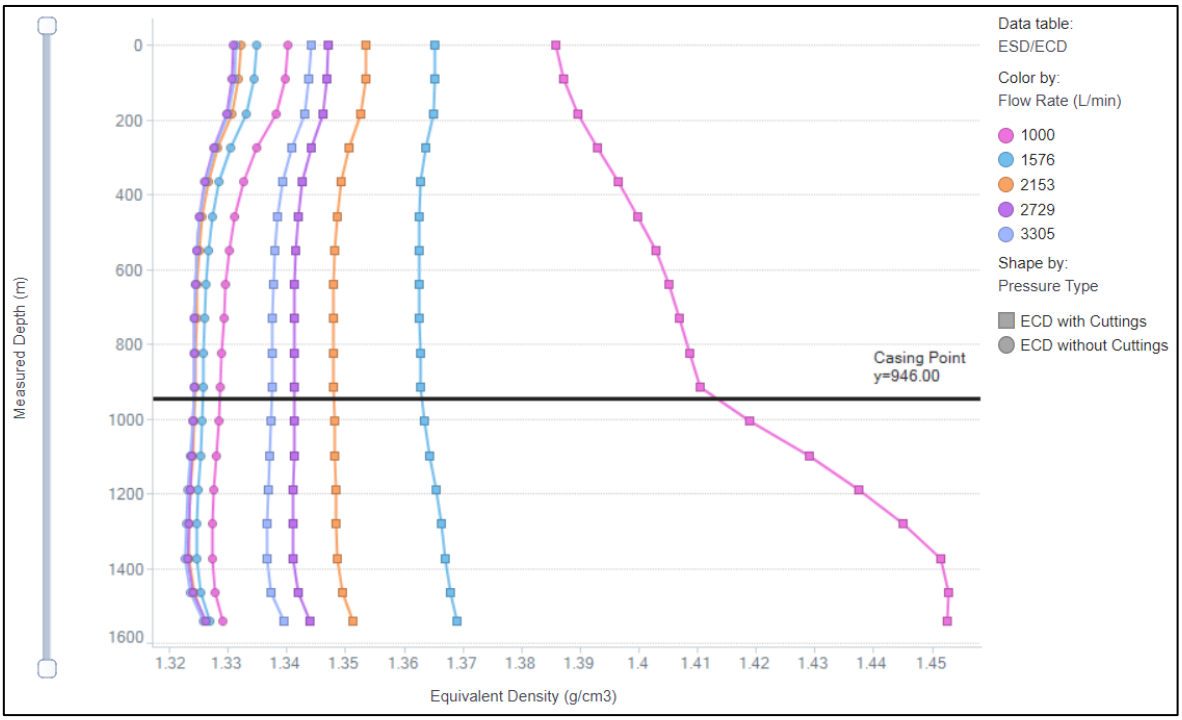

Figure 2.11 - Measured depth vs Equivalent density, with very different flow rates. Squared points illustrates ECD with cuttings, while circle points show ECD without cuttings. In this example, low flow rate clearly increases ECD. ROP is set to 20 m/h. Bit rotation is 120 RPM. For this drilled section, well inclination is 0° at start depth and 12.7° at end measured depth.

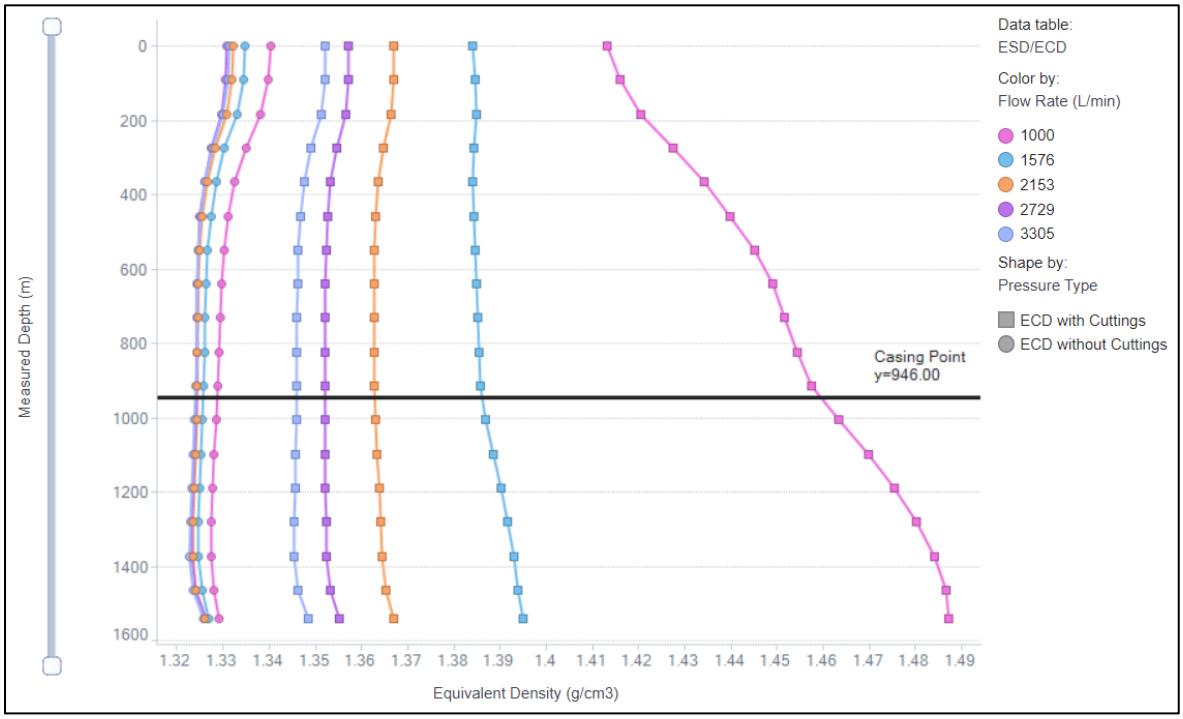

Figure 2.12 - Measured depth vs Equivalent density, with very different flow rates. Squared points illustrates ECD with cuttings, while circled points show ECD without cuttings. In this example, low flow rate clearly increases ECD. ROP is set to 33 m/h. Bit rotation is 120 RPM. For this drilled section, well inclination is 0° at start depth and 12.7° at end measured depth.

2.3 Pressure- and temperature effects on drilling fluids

To accurately calculate hydraulics of oil-well drilling fluids, it is important to consider the downhole behavior of fluid properties. Downhole, the viscosity and density of the drilling fluid are dependent on dynamic and static temperature, as well as pressure. For especially oil- and synthetic-based drilling fluids, it is important to consider the fluid properties downhole, since these rheological properties can be significantly different from those measured at surface conditions. Hence, there exists a limitation of the usefulness of hydraulics calculations made with surface-measured rheological parameters [9].

2.3.1 Pressure- and temperature effects on drilling fluids viscosity

When pressure- and temperature effects on rheological properties are considered separately, the downhole effects can be summarized as follows [9]:

- Pressure usually increases the viscosity of drilling fluids.
- The viscosity of oil-well drilling fluids will generally decrease with increasing temperature.

While the pressure effects on drilling fluid viscosity are normally exponential, temperature effects on drilling fluid viscosity are typically non-linear. The combined pressure- and temperature effects on drilling fluids alter from one fluid type to another, i.e., the effects depend on the fluid type. Pressure- and temperature effects on viscosity are most pronounced for non-aqueous drilling fluids. *Figure 2.13* illustrates viscosity profiles for three different non-aqueous based fluids as a function of temperature. As a result of increasing temperature, a clearly non-linear viscosity reduction can be seen [9].

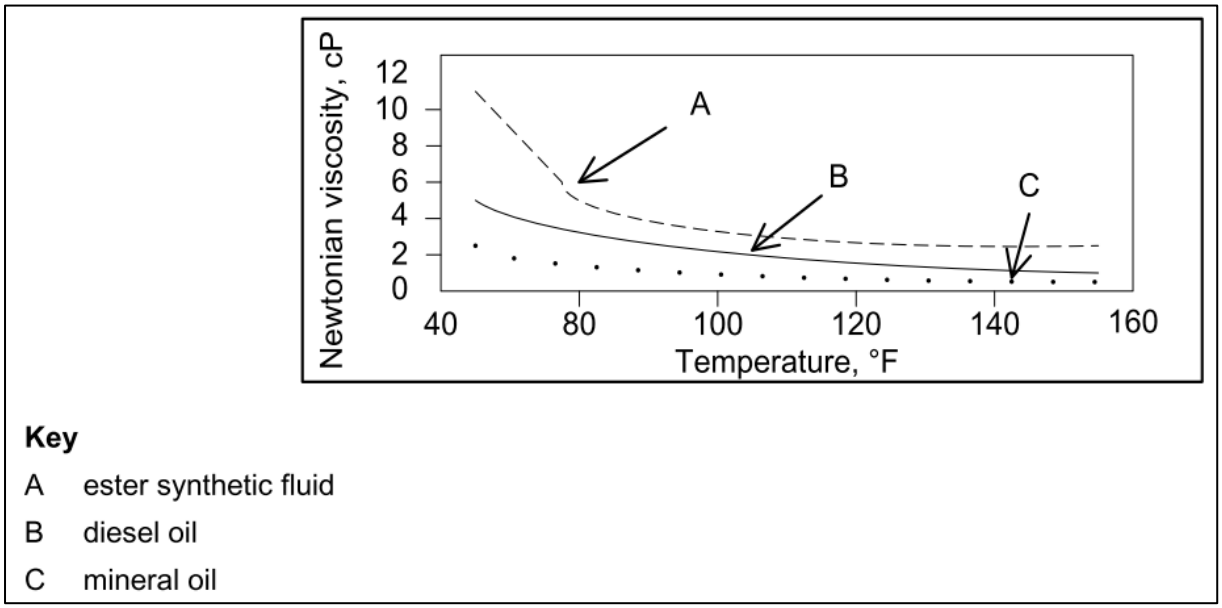

Figure 2.13 – Viscosity as a function of temperature for three non-aqueous base fluids. Source: [9]

Rommetveit and Bjorkevoll investigated and compared how pressure and temperature effected viscosity for water based mud (WBM) and oil based mud (OBM) [26]. The pressure effect was much less decisive than the temperature effect on WBM. Compared to WBM, the pressure dependence was much more pronounced for OBM. When pressure increased from atmospheric to 1000 bar and temperature increased from 50°C to 150°C in their OBM experiments, the pressure and temperature effects almost cancelled each other [26].

2.3.2 Pressure- and temperature effects on drilling fluids density

By separately considering the pressure- and temperature downhole effects on drilling fluids density, one can summarize the following [9]:

- Normally, pressure serve to increase drilling fluid density.
- Increasing temperature generally decreases the drilling fluid density.

Pressure effects on drilling fluids density are usually linear at high pressures, whereas the temperature effect on non-aqueous drilling fluids density mostly is near-linear or linear. The combined pressure and temperature effect on density will as for the viscosity effect also depend on which drilling fluid type is used, i.e., the composition of the fluid. Pressure- and temperature effects on density are most pronounced for invert emulsions and completely non-aqueous drilling fluids. *Figure 2.14* shows how a synthetic-based drilling fluid density are affected by pressure and temperature [9].

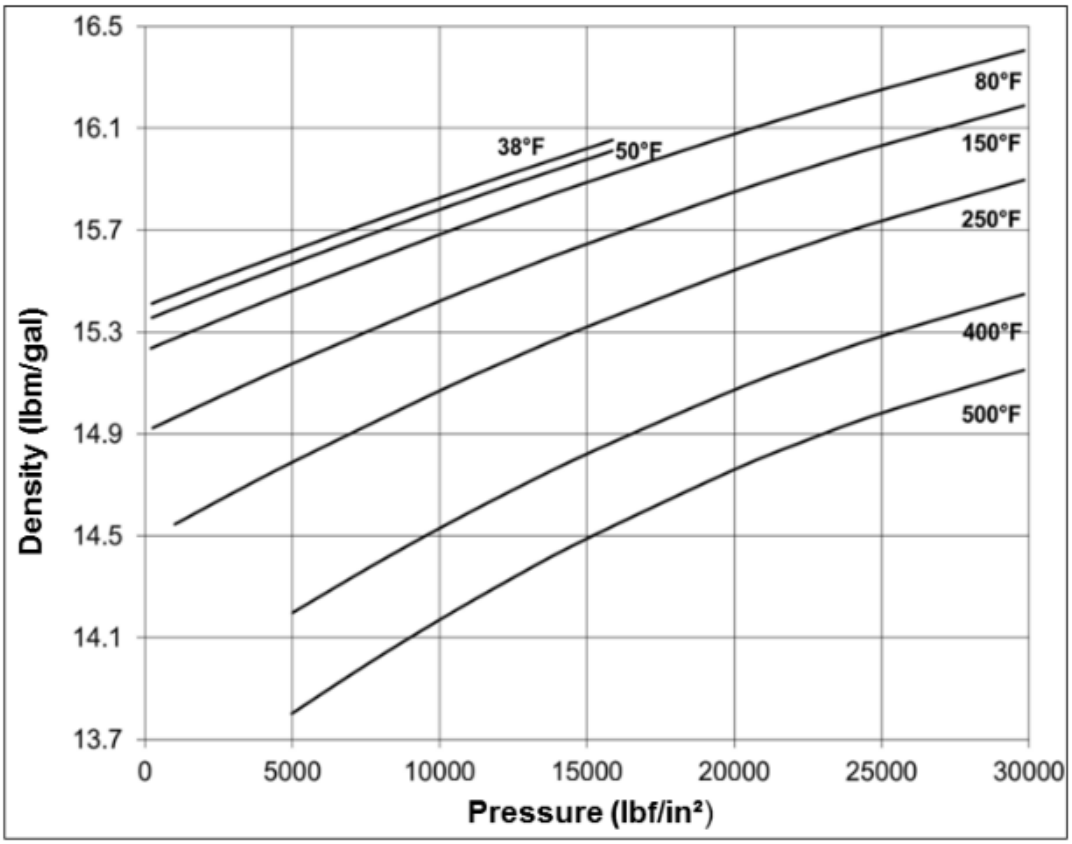

Figure 2.14 – Synthetic-based drilling fluid density under different pressure and temperature. Source: [9]

Rommetveit and Bjorkevoll states that the density of water- and oil based drilling fluids are clearly dependent on the position in the wellbore [26]. Water based drilling fluid density has a greater temperature dependence than an oil based drilling fluid density, but a less pressure dependency [26].

2.4 Flow regimes

Different types of flow regimes influence a fluids performance function due to different behavior. Factors like viscosity, density, fluid velocity, size- and shape of the flow channel help to distinguish between the flow regimes. The different flow regimes are laminar, transitional and turbulent [9]. *Figure 2.15* illustrates these regimes.

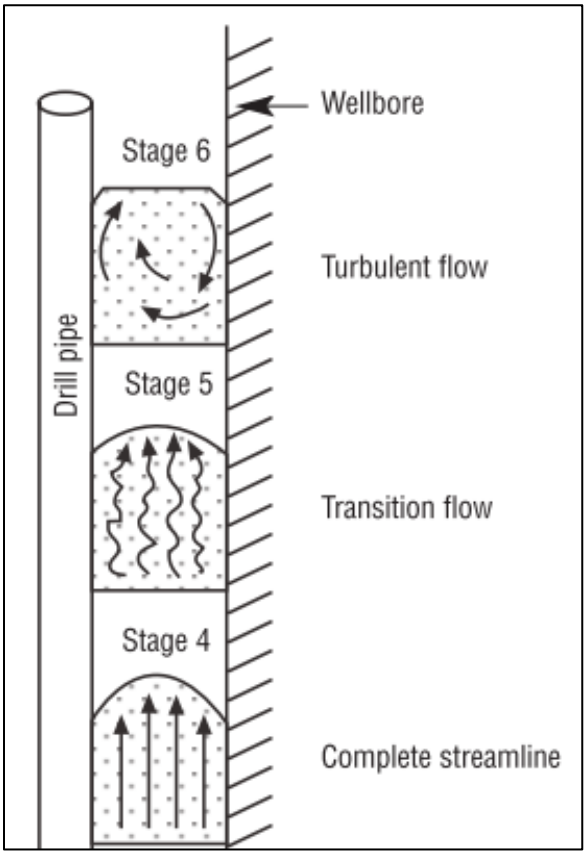

Figure 2.15 - Flow regimes:
Stage 4 - laminar flow. Stage 5 - transitional flow. Stage 6 - turbulent flow.
Source: [6]

2.4.1 Laminar flow

A fluid will in laminar regime move parallel to the walls of the flow channel in smooth lines. If the moving fluid is viscous and/or moving slowly, the flow regime tends to be laminar. In a laminar flow, the required pressure in order to move the fluid will increase with increasing viscosity and velocity [9]. For Newtonian fluids in laminar flow, pressure drop increases linearly with velocity and viscosity. This is not the case for Herschel-Bulkley fluids in laminar flow, due to the yield stress and shear thinning [27].

2.4.2 Transitional flow

Relative contributions of inertial and viscous forces in a flow controls the transition from laminar flow to turbulent flow. Laminar flow is dominated by the viscous forces. On the other hand, the inertial forces play a more significant role in turbulent flow. Viscous forces vary linearly with the flow rate for Newtonian fluids, unlike the inertial forces that vary as the square of flow rate [9].

Reynolds number, N_{Re}, is the ratio of the inertial forces to viscous forces and can be seen in *Equation 2.11* [9].

Equation 2.11 - Reynolds number:

$$N_{Re} = \frac{\rho V d}{\mu} \qquad 2.11$$

Where (in SI units):

N_{Re} – Reynolds number

ρ – fluid density $\left(\frac{kg}{m^3}\right)$

V – average flow velocity $\left(\frac{m}{s}\right)$

d – diameter of the flow channel (m)
circular pipe/tube: d = inside diameter
annulus: d = hydraulic diameter (outer hole diameter - inside diameter of inner pipe)

μ – fluid viscosity $(Pa \cdot s)$

The critical velocity is where the transition from laminar flow to transitional flow occurs. For common drilling fluids, this usually occurs over a range of velocities corresponding to Reynolds numbers between 2000 and 4000 [9].

2.4.3 Turbulent flow

In a turbulent regime, the bulk of fluid moves forward, but the fluid flow is eddying and swirling as it moves along flow channel. Velocity fluctuations can arise spontaneously in this regime. The amount of turbulence can rise, depending on wall roughness and the rapid alterations in flow directions. If a moving fluid exhibits low viscosity and/or high flow velocity, it often tends to be in a turbulent flow. The pressure required to move the fluid rise linearly with density and roughly with the square of the velocity. In other words, a higher pump pressure is required in order to move a fluid in a turbulent flow compared to in a laminar flow [9].

2.5 Pressure losses in a circulating system

This thesis will focus on annular pressure losses, i.e., pressure losses that occurs after the drilling fluid has exited the drill bit, since other pressure losses will not have an impact on equivalent circulating density (ECD). Annular pressure losses will be further introduced from chapter *2.5.1 Concentric annular pressure losses* until end of chapter *2.5.3 Annular pressure losses with drill string rotation.*

Knowledge about pressure losses in a drilling system is important for planning, hydraulic analysis, and optimization. Information about pressure losses is also needed for modeling special well-construction operations like well control, tripping, cementing, and casing runs. [9].

In a circulation system, the pump pressure (P_p) is equal to the sum of surface back pressure, frictional pressure losses and hydrostatic pressure difference between the annulus and drill string. Whereas the bottomhole pressure (P_{bh}) in a well is the sum of surface back pressure, the annular frictional pressure losses, and the annular hydrostatic pressure. The pump pressure and the bottomhole pressure can be calculated using *Equation* 2.12 and *Equation 2.13*, respectively. These equations are applicable to synthetic-, oil-, and water based fluids, but they do not address foam, gas, air and other aerated or highly compressible fluid [9]. *Figure 2.16* illustrates a simplified circulation system.

Equation 2.12 - Pump pressure:

$$P_p = P_{sc} + P_{ds} + P_{dt} + P_b + P_a + P_{cl} + P_c + P_{ha} - P_{hd} \qquad 2.12$$

Where (in SI units):

P_p – pump pressure (Pa)

P_{sc} – surface-connections pressure loss (Pa)

P_{ds} – drill string pressure loss (Pa)

P_{dt} – downhole tools + motors pressure loss (Pa)

P_b – bit pressure loss (Pa)

P_a – annular pressure loss (Pa)

P_{cl} – choke line pressure loss (Pa)

P_c – casing pressure, back pressure on annulus (Pa)

P_{ha} – annular hydrostatic pressure (Pa)

P_{hd} – drill string hydrostatic pressure (Pa)

Equation 2.13 - Bottomhole pressure:

$$P_{bh} = P_a + P_{cl} + P_c + P_{ha} \qquad 2.13$$

Where (in SI units):

P_{bh} – bottomhole pressure (Pa)

P_a – annular pressure loss (Pa)

P_{cl} – choke line pressure loss (Pa)

P_c – casing pressure, back pressure on annulus (Pa)

P_{ha} – annular hydrostatic pressure (Pa)

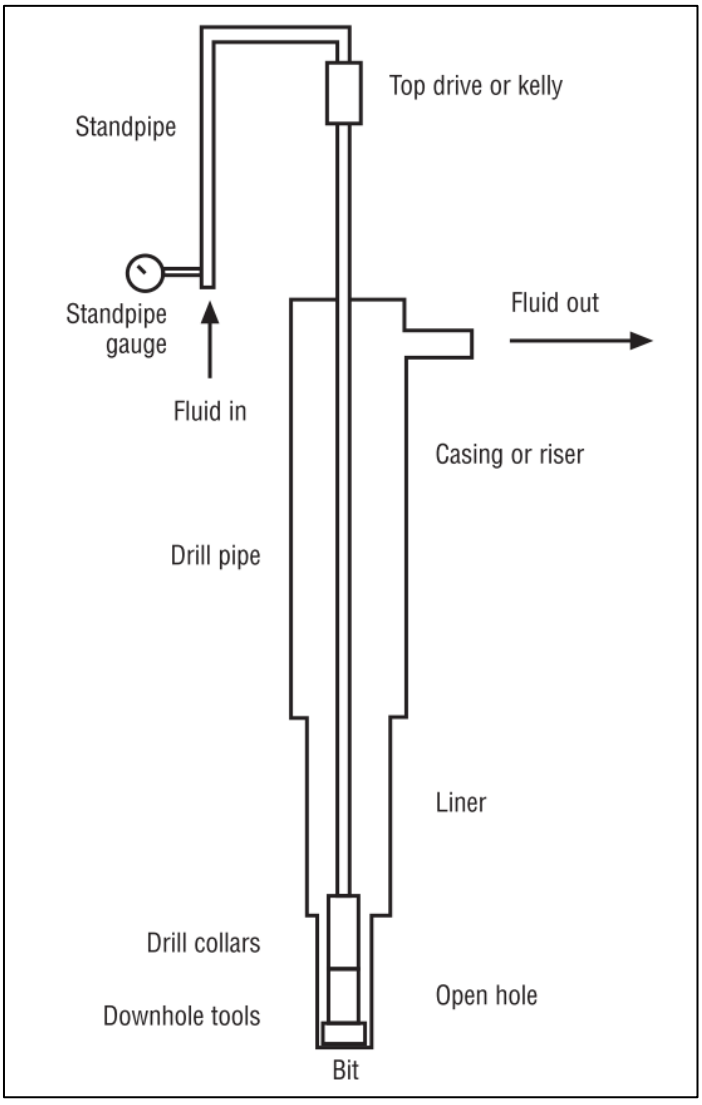

Figure 2.16 - Simplified illustration of a circulating system. Source:[6]

2.5.1 Concentric annular pressure losses

In 2008 it was presented a methodology for predicting pressure drop for laminar, transitional and turbulent flow for Herschel-Bulkley fluids in concentric annuli [28]. Founargiotakis et al. used the slot model in their work in order to approximate flows in concentric annuli [28]. Flow in annulus can be approximated using equations established for flow through rectangular slots. If the ratio of the outside radius of the pipe and the wellbore radius is greater than 0.3, the slot equations are reasonably accurate and much simpler to use [8]. *Figure 2.17* illustrates the flow in annulus as a slot for a Herschel-Bulkley fluid.

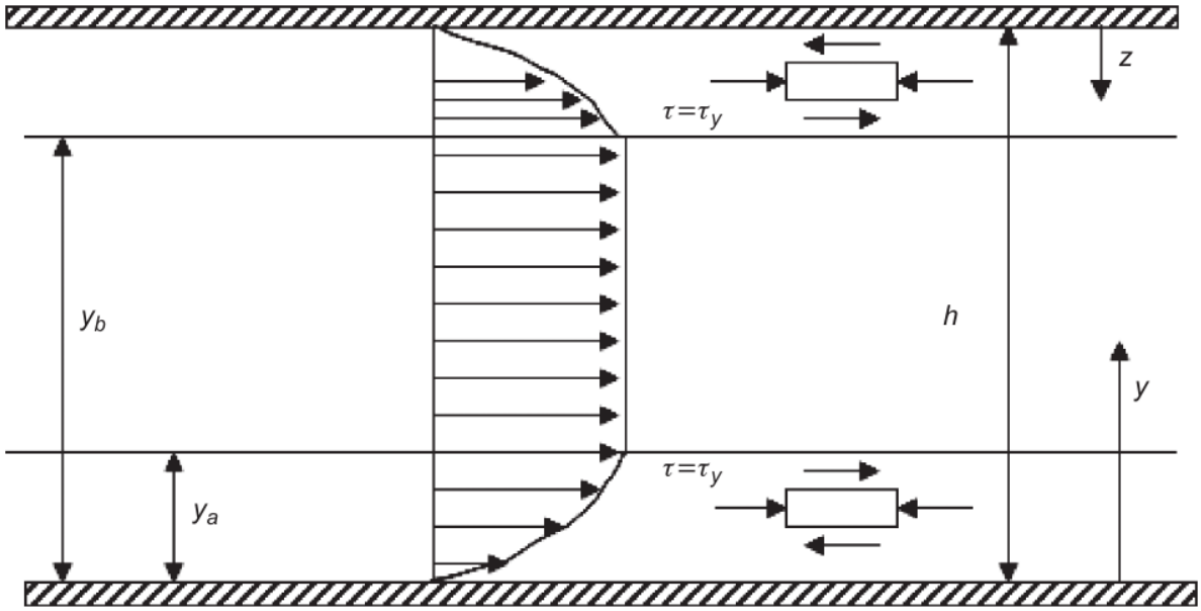

Figure 2.17 – Flow in annulus using the slot model for a Herschel-Bulkley fluid. Source: [8]

Founargiotakis et al. converted the Herschel-Bulkley model rheological behavior to an equivalent power-law rheological model [28]. They then used the power-law definition of Reynolds number, and the Fanning friction factor [28].

Equation 2.14 - Consistency index of equivalent power-law rheological behavior:

$$K' = \frac{\tau_y + K\left(\left(\frac{2n'+1}{3n'}\right)\dot{\gamma}_{Nw}\right)^{n}}{(\dot{\gamma}_{Nw})^{n'}} \qquad 2.14$$

Equation 2.15 - Flow index of equivalent power-law rheological behavior:

$$n' = \frac{n(1-\xi)(n\xi + n + 1)}{1 + n + 2n\xi + 2n^2\xi^2} \quad 2.15$$

Where the dimensionless shear stress, $\xi = \frac{\tau_y}{\tau_w} = \frac{2\tau_y}{h\left(\frac{dp}{ds}\right)_c}$ and $\left(\frac{dp}{ds}\right)_c$ is the pressure drop gradient.

Furthermore, a generalized Herschel-Bulkley Reynolds number got defined as [28]:

Equation 2.16 - Generalized Herschel-Bulkley Reynolds number:

$$Re' = \frac{\rho_f (2h)^{n'} \overline{v}_f^{(2-n')}}{K' 12^{(n'-1)}} \quad 2.16$$

Where ρ_f is the fluid mass density, $h = \frac{d_w - d_o}{2}$ is the annulus thickness calculated using wellbore diameter d_w and the pipe outer diameter d_o. $\overline{v}_f$ is the bulk fluid velocity. The boundaries for laminar and turbulent flow are dependent on n', and they are defined as [28]:

- $Re'_{laminar} = Re' < 3250 - 1150n'$
- $Re'_{turbulent} = Re' > 4150 - 1150n'$

If the flow is laminar, it is possible to solve numerically *Equation 2.17* to obtain the pressure loss gradient [28].

Equation 2.17 - Concentric annular pressure loss for laminar flow:

$$Q = \left(\frac{\left(\frac{dp}{ds}\right)_c}{K} \right)^m \frac{2W\left(\frac{h}{2}\right)^{m+2}(1-\xi)^{m+1}}{(m+1)(m+2)}\left(\xi + (m+1)\right) \quad 2.17$$

Where the flow rate is Q, $W = \frac{\pi\left(d_w^2 - d_o^2\right)}{4h}$ and $m = \frac{1}{n}$.

On the other hand, if the flow is turbulent, the pressure loss can be estimated through a Fanning friction factor, $f_{Fanning}$ in *Equation 2.18* [28].

Equation 2.18 - Concentric annular pressure loss for turbulent flow:

$$f_{Fanning} = \frac{h}{\rho_f \overline{v}_f^2}\left(\frac{dp}{ds}\right)_c \quad 2.18$$

The Fanning friction factor for Herschel-Bulkley fluid in *Equation 2.19* got estimated and defined by Founargiotakis et al. [28].

Equation 2.19 - Estimated Fanning friction factor:

$$\frac{1}{\sqrt{f_{Fanning}}} = \frac{4}{n'^{0.75}} log_{10}\left(Re' f_{Fanning}^{1-\frac{n'}{2}}\right) - \frac{0.395}{n'^{1.2}} \quad 2.19$$

For the transitional flow, the transitional friction factor is estimated by linear interpolation since no other interpolation approaches have proven to provide better estimates. *Equation 2.20* shows the estimated transitional friction factor [28]:

Equation 2.20 - Estimated transitional friction factor:

$$f_{tr} = f_l + \frac{(Re' - Re'_{laminar})(f_t - f_l)}{Re'_{turbulent} - Re'_{laminar}} \quad 2.20$$

Where f_t is the result of *Equation 2.19* with the Reynolds number $Re'_{turbulent}$ and $f_l = \frac{24}{\mathrm{Re}'_{\mathrm{laminar}}}$.

Founargiotakis et al. provided semi-analytical solutions for transitional- and turbulent flows by using a local power-law approach that gave equations which related local power law parameters, K' and n', to the annulus flow geometry and to the rheological parameters of Herschel-Bulkley model [28].

In laminar-, transitional- and turbulent flow the shear stress at the wall τ_w, can be calculated using *Equation 2.21* [8].

Equation 2.21 - Shear stress at the wall:

$$\tau_w = \frac{h}{2}\left(\frac{dp}{ds}\right)_c \quad 2.21$$

For turbulent flow, *Equation 2.21* will give the average shear stress, $\bar{\tau}_w$, due to fluctuations in the shear stress along the wall.

2.5.2 Eccentric annular pressure losses

For accurate prediction of equivalent circulating density (ECD), eccentricity should be considered, since it has been shown that drill pipe eccentricity can significantly reduce annular pressure losses [29]. Even in slightly deviated wells, the inner pipe is rarely concentrically located inside the flow geometry. In other words, it exists eccentricity in almost all wells. The eccentricity must be considered in order to avoid inaccurate concentric annuli assumptions.

Eccentricity is defined by *Equation 2.22*. A eccentricity e-value equal to one indicates a fully eccentric annulus, while a e-value equal to zero describes concentric annulus [30]. An illustration of an eccentric annulus can be seen in *Figure 2.18*.

Equation 2.22 - Eccentricity:

$$e = \frac{2\delta}{d_o - d_i} \qquad 2.22$$

Where (in SI units):

$e -$ eccentricity

$\delta -$ distance between centers of inner and outer pipes (m)

$d_o -$ outer pipe diameter (m)

$d_i -$ inner pipe diameter (m)

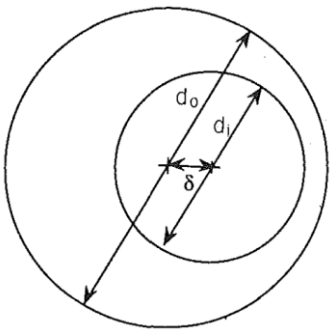

Figure 2.18 - Eccentric annulus.
Source: [30]

Cayeux describes a problem with numerical stability of solutions to the flow in eccentric annulus [31]. Due to numerical problems when approaching plug zones, the solvers converge slowly, as erratic oscillations in the effective viscosity persist for long periods. Hence such solutions are far too slow and computer intensive for real-time applications [31].

Correlations can be used to consider the eccentricity effect. In 1990 Haciislamoglu and Langlinais introduced a correlation that consider eccentricity for power-law fluids in laminar flow, $R_{(pl)l}$ [30]. Four years later in 1994, Haciislamoglu and Cartalos published a fairly similar correlation for power-law fluids in turbulent flow, $R_{(pl)t}$ [32]. The correlations for power law fluids in laminar- and turbulent flow can be seen below in *Equation 2.23* [30] and *Equation 2.24* [32], respectively.

Equation 2.23 - Correlation from concentric to eccentric conditions for power-law fluids in laminar flow:

$$R_{(pl)l} = 1 - 0.072\frac{e_{avg}}{n}\left(\frac{d_i}{d_o}\right)^{0.8454} - 1.5e_{avg}^2\sqrt{n}\left(\frac{d_i}{d_o}\right)^{0.1852} + 0.96e_{avg}^3\sqrt{n}\left(\frac{d_i}{d_o}\right)^{0.2527} \quad 2.23$$

Equation 2.24 - Correlation from concentric to eccentric conditions for power-law fluids in turbulent flow:

$$R_{(pl)t} = 1 - 0.048\frac{e_{avg}}{n}\left(\frac{d_i}{d_o}\right)^{0.8454} - \frac{2}{3}e_{avg}^2\sqrt{n}\left(\frac{d_i}{d_o}\right)^{0.1852} + 0.285e_{avg}^3\sqrt{n}\left(\frac{d_i}{d_o}\right)^{0.2527} \quad 2.24$$

The frictional pressure loss gradient in an eccentric annulus can be calculated by *Equation 2.25* [30].

Equation 2.25 – Frictional pressure loss gradient in an eccentric annulus:

$$\left(\frac{dp}{ds}\right)_e \approx \left(\frac{dp}{ds}\right)_c R_{(pl)} \quad 2.25$$

Where $\left(\frac{\mathrm{dp}}{\mathrm{ds}}\right)_{\mathrm{e}}$ is the frictional pressure loss gradient in an eccentric annulus, $\left(\frac{\mathrm{dp}}{\mathrm{ds}}\right)_{\mathrm{c}}$ is the frictional pressure loss gradient in concentric annulus and $R_{(pl)}$ is the correlation, which will be $R_{(pl)l}$ or $R_{(pl)t}$. $R_{(pl)l}$ correlation is used for laminar flow, while $R_{(pl)t}$ is used for turbulent flow. *Figure 2.19* illustrates $R_{(pl)}$ at different eccentricities ranging from 0 to 0.9. In addition, the figure shows how the shear thinning exponent, n, influences the frictional pressure at a given eccentricity. Increased shear thinning gives a lower reduction in frictional pressure at a given eccentricity for both laminar- and turbulent conditions.

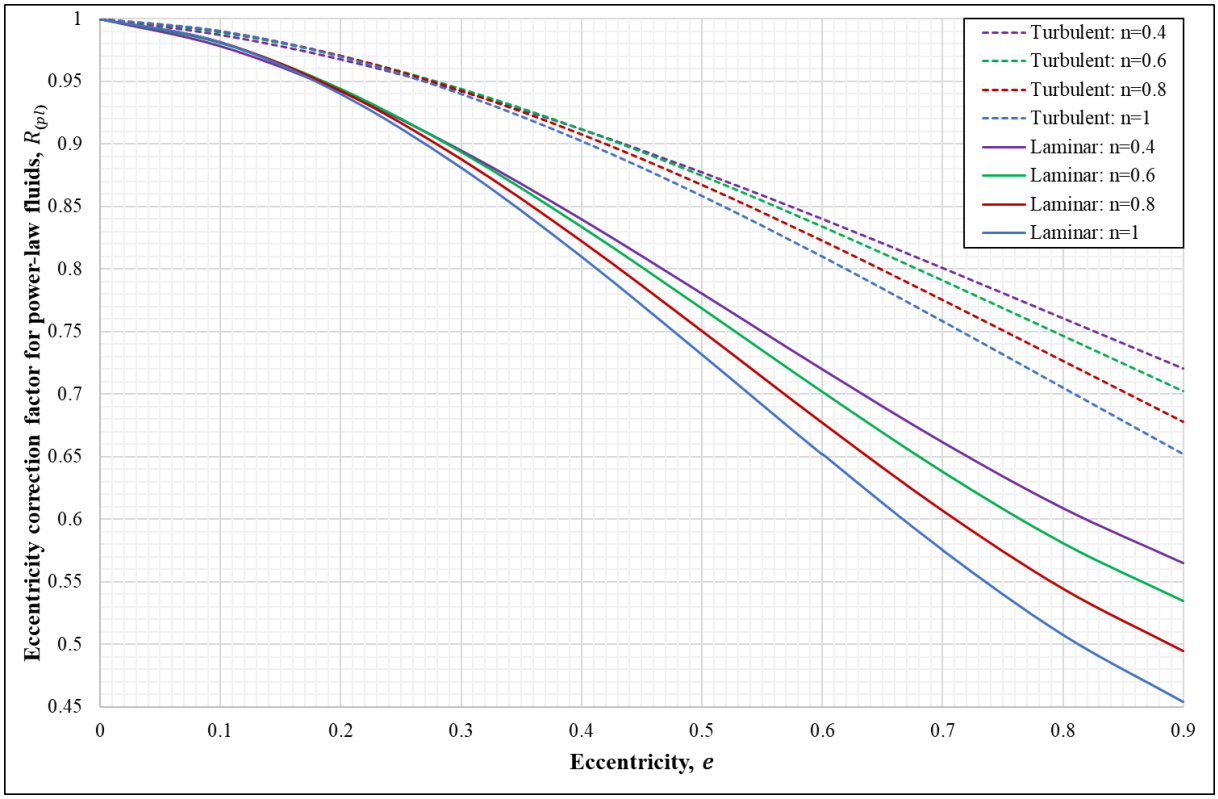

Figure 2.19 - Eccentricity correction factor for power-law fluids vs eccentricity, with variation in the shear thinning exponent.

Regarding the transitional flow, a linear interpolation based on the generalized Reynold number is made between the calculated values for turbulent and laminar conditions [31].

Dokhani et al. emphasized that the correlation proposed by Haciislamoglu and Cartalos [32] specifically was developed for power-law fluids [29]. By this reason, they may not be applied for fluids that exhibit yield behavior. Unfortunately, several researchers have used this correlation to correct for the effect on eccentricity in presence of yield-power fluid. This have provided enough motivation to Dokhani et al. to revisit the flow of non-Newtonian fluids in eccentric annuli. They published a paper with an updated correlation to be applicable for yield-power-law (known as Herschel-Bulkley) fluids in laminar flow for prediction of frictional pressure losses in eccentric annuli. Dokhani et al. fitted a polynomial equation using non-linear regression analysis after 286 different scenarios were simulated. Their new proposed correlation can be seen in *Equation 2.26* [29].

Equation 2.26 - Correlation from concentric to eccentric conditions for Herschel-Bulkley fluids in laminar flow:

$$R_{HB} = 1 - 0.082\frac{e}{n}S^{1.502} - 1.57e^2\sqrt{n}S^{0.44} + 0.975e^3\sqrt{n}S^{0.597} + 0.0735e^2\tau_o^{0.408} \qquad 2.26$$

Where S is the ratio of inner and outer pipe diameter, and τ_o is the dimensionless normalized yield point which is defined as $\tau_0 = \frac{\tau_y}{\tau_c}$, where τ_c is constant and chosen as $5\ \frac{lbf}{100\ ft^2}$ [29].

The new correlation R_{HB} got compared to Haciislamoglu and Cartalos correlation [29]. This comparison can be seen in *Figure 2.20.*

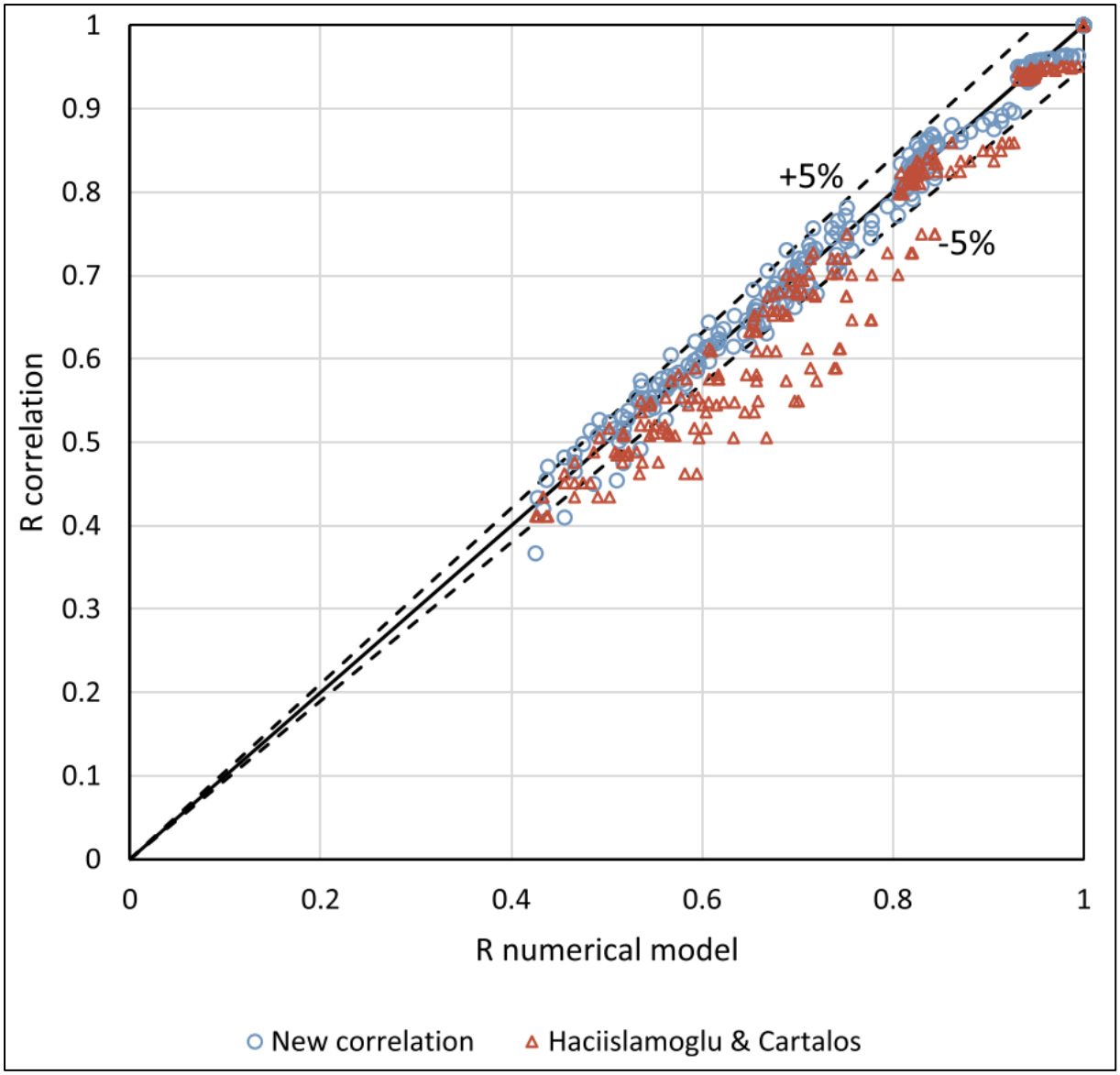

Figure 2.20 - Dokhani et al. correlation compared with Haciislamoglu and Cartalos correlation. The X-axis corresponds to R-value from numerical simulations, while Y-axis corresponds to the two R-correlations proposed. Solid black line indicates a perfect fit. Source: [29]

Dokhani et al. discovered that Haciislamoglu and Cartalos under-predicts the frictional pressure losses for fluids that exhibit yield behavior. Furthermore, they concluded that recent developed correlation is applicable in order to get a more accurate estimate of ECD [29].

2.5.3 Annular pressure losses with drill string rotation

The effect of drill string rotation on annular pressure losses is a complicated topic. Literature shows some inequalities in different observations regarding laboratory findings and actual field results. In 2014, Saasen published an overview paper of research findings regarding the effect on drill string rotation on annular frictional pressure losses [33].

At the laboratory, positive and negative effects of the inner pipe rotation speed have been seen [33]. Newtonian and non-Newtonian fluids have in a concentric annulus showed an increase in the friction factor with inner pipe rotation compared to a non-rotating case for flow in laminar regime. Through another experimental study, where the effect of both rotation and eccentricity was investigated, non-Newtonian fluids that best fitted the power-law model showed unexpected pressure loss pattern. From this study one could confirm that that pressure losses could decrease or increase as pipe rotation increases. On the other hand, another study conducted with diameter ratio 80% and partially 50% eccentric annulus showed mainly an increased annular pressure loss with increasing rotational speed. Furthermore, others have again shown that annular pressure loss indeed could possibly decrease or increase as the drill pipe rotation speed increase [33].

Saasen's review paper also shows ten field measurements, whereas nine of them indicates a significant increase in pressure losses as the drill string rotation increases [33]. A field study from the North Sea area observed a significantly lower pressure loss than modelled by standard models in absence of rotation. The lower pressure loss was most likely due to an eccentric annulus. Anyhow, when the rotation was added, the pressure loss was increased back to the modelled prediction, meaning the rotation increased the annular pressure loss. Another study from the North Sea also showed similar results, indicating credible findings. Field studies have shown that rotation from 0 RPM to 60 RPM gives a sharp increase in annular pressure loss, while the increase in pressure loss was less pronounced when the rotation rate continued to increase up to 120 RPM. One of the ten field measurements had opposite results and showed reduction in annular frictional pressure losses with increased rotation [33].

Factors like irregular geometry of the wellbore, drill pipe wobbling or instability, operating with multiple dimension scales, too simple fluid systems in the laboratory, tool joint effect or just a combination of these above-mentioned factors, can attribute to the discrepancy between field- and lab findings [33]. The effect of drill string rotation on frictional annular pressure losses is a complicated inconsistent subject. Rotation can probably decrease or increase the frictional annular pressure losses, depending on the prevailing conditions.

Cayeux says that the decrease of the apparent viscosity of yield stress power-law fluid with increasing shear stress is the reason for possible decrease of pressure losses with drill string rotation [31]. Anyhow, inertial effects dominate, and the pressure losses increase again when a certain level of rotational speed is passed. Centrifugal force causes inertial effects that applies to drilling fluids when displaced radially. This can initiate Taylor vortices. Cayeux further says that with sufficient pipe eccentricity, experimental- and numerical studies demonstrates that the frictional pressure loss always increase for all rotational speed. Due to this fact, he introduced a rotation specific correlation correction that can obtain an estimation of the pressure loss gradient in an eccentric configuration with drill pipe rotation. *Equation 2.27* shows the rotation correction correlation, R_{rot} [31], while *Figure 2.21* describe R_{rot} graphically.

Equation 2.27 - Rotation correction correlation:

$$R_{rot} = 1 + max\left(0, 1.639 - \frac{394.63}{Re'}\right)\frac{\sqrt{Ta}}{Re'} \qquad 2.27$$

Ta is the Taylor number and can be seen in *Equation 2.28*, while Re' can be seen in *Equation 2.16* [31].

Equation 2.28 - Taylor number:

$$Ta = \frac{d_o(d_w - d_o)^3}{16}\left(\frac{\rho_f \dot{\theta}}{2\pi\mu_{eff}}\right)^2 \qquad 2.28$$

Where $\mu_{eff} = \frac{\tau}{\gamma}$ is the effective viscosity and $\dot{\theta}$ is the angular rotational speed. Using experimental data, *Equation 2.27* got derived. The Reynolds number was comprised between 10 and 2000, while the Taylor number varied between 0 and 420 000. Thus the estimation of the pressure loss gradient in an eccentric configuration with drill string rotation, $\left(\frac{dp}{ds}\right)_{e+rot}$, can be seen in *Equation 2.29* [31].

Equation 2.29 – Pressure loss gradient including eccentricity and drill string rotation:

$$\left(\frac{dp}{ds}\right)_{e+rot} \approx R_{rot} R_{(pl)} \left(\frac{dp}{ds}\right)_c \qquad 2.29$$

The difference between *Equation 2.29* and *Equation 2.25* is the rotation correction correlation, R_{rot}.

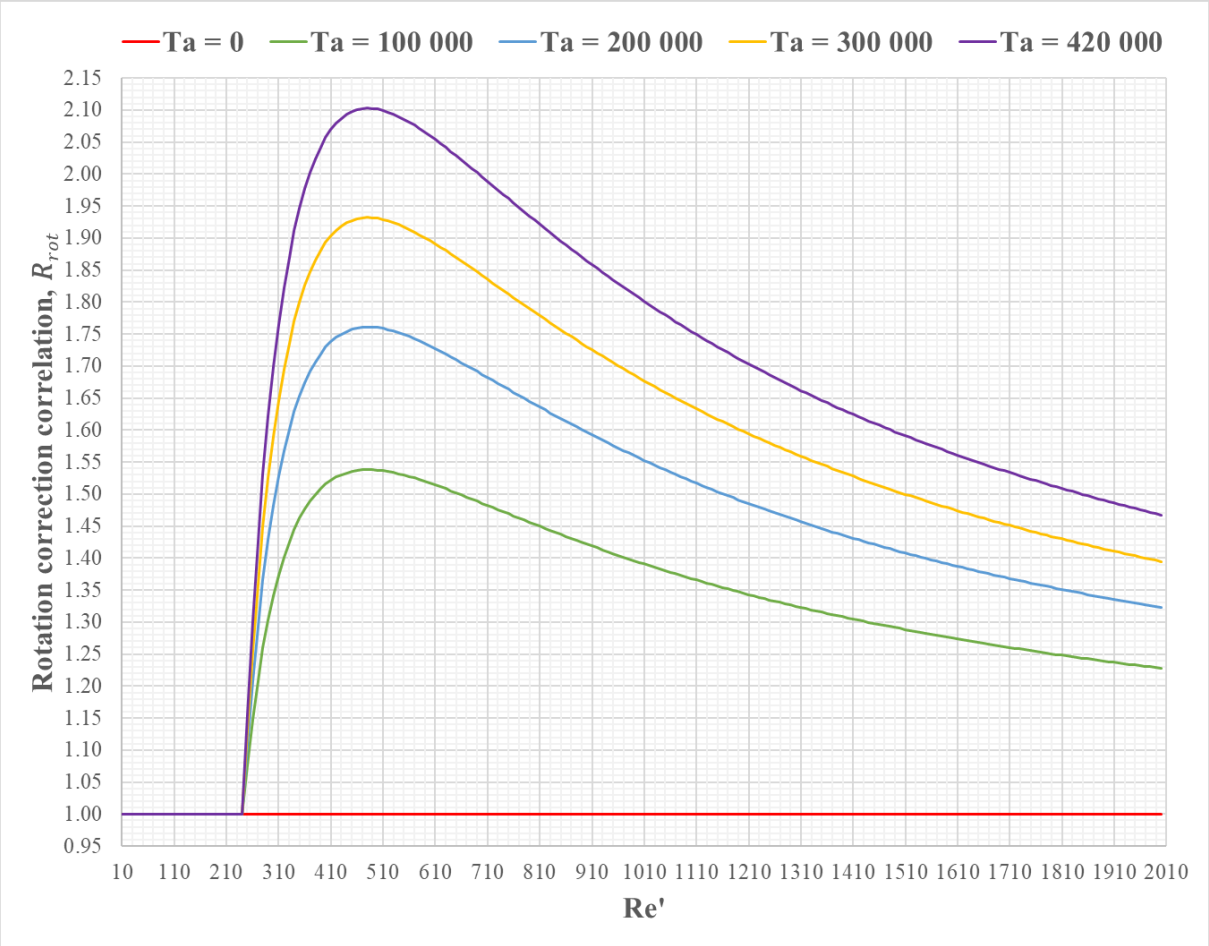

Figure 2.21 - Rotation correction correlation, R_{rot} as a function of Re' values between 10 and 2000, for five different Taylor numbers. R_{rot} correlation is greatest for large Ta-values.

3. Method and implementation

Schlumberger's digital well construction solution, DrillPlan, was used to simulate the equivalent circulating density calculations. Necessary well data and parameters were entered into the software, before detailed sensitivity analysis was performed in the background. The results were exported as CSV-files and placed in a folder structure for further analysis using Microsoft Excel. Using Queries & Connections in Microsoft Excel, the sensitivity-data from DrillPlan simulations were filtered, adjusted, formatted, and plotted accordingly to the plan. At the very end, the resulting tables and figures were inserted to the thesis.

3.1 Hydraulic Analysis in DrillPlan

In hydraulic analysis, DrillPlan uses the Herschel-Bulkley model for drilling fluid rheology [34]. DrillPlan takes account of the function of temperature and pressure when calculating the downhole rheology and fluid density. Calculations of equivalent circulating density (ECD) and annular pressure drop are based on American Petroleum Institute Recommended Practice 13D (API RP 13D) (this thesis source: [9]), with correction for the effect of revolutions per minute (RPM), i.e., drill string rotation. Additionally, the eccentricity correction work of Haciislamoglu and Cartalos is included (this thesis source: [32]) for eccentricity correction. Note that the maximum eccentricity is defined with an assumption that the tool joints always are in touch with the borehole. Other calculations performed in DrillPlan are motor/turbine bearings, hole-opener/under-reamer nozzles, and flow split through an unlimited number of bypass tools. Automatically, the hydraulic analysis takes account of the pilot hole diameter beneath any hole openers or under-reamers since it uses drill hole diameter from various tools to determine the hole size. Furthermore, bit pressure drop is in accordance with API RP 13D, while motor power curves are based on published specifications, as defined in bottom hole assembly tool properties [34].

DrillPlan's hydraulic analysis also uses several default inputs. These are introduced below [34]:

- The low shear yield point (LSYP) is defaulted according to the API yield point and mud type, with a multiplier as WBM = 0.30 / OBM = 0.50 / SBM = 0.57.
- Surface equipment: 3.83 $inches$ inside diameter, 146 m.
- Tool joint length fraction is based on the pipe tool joint properties in bottom hole assembly (BHA) or default to 10% pipe length.
- Cuttings: Cutting type, cutting size and cutting density are based on user input.

Other calculation inputs needed in DrillPlan for hydraulic calculations are the following design or context objects; rig, wellbore geometry, trajectory, drilling parameters, drilling fluid properties and BHA/drill string [34].

3.2 Well selection

Three anonymized deviated wells from the North Sea were investigated in this study. The explored wells have been given the names Loris-234, Loris-345 and Loris-567. These wells were selected as they are representative of typical well designs, and they were drilled recently. Additionally, the drilling parameters and downhole ECD data were available. All wells are drilled from a platform, and they are sidetracks from existing wellbores. The sections were drilled with oil based drilling fluids. All drilled sections except Loris-567_6in have used a drilling fluid system named Versatec. In the Loris-567_in section, the OB WARP drilling fluid system was used. The trajectories of the wellbores can be seen in *Figure 3.1, Figure 3.2* and *Figure 3.3* below.

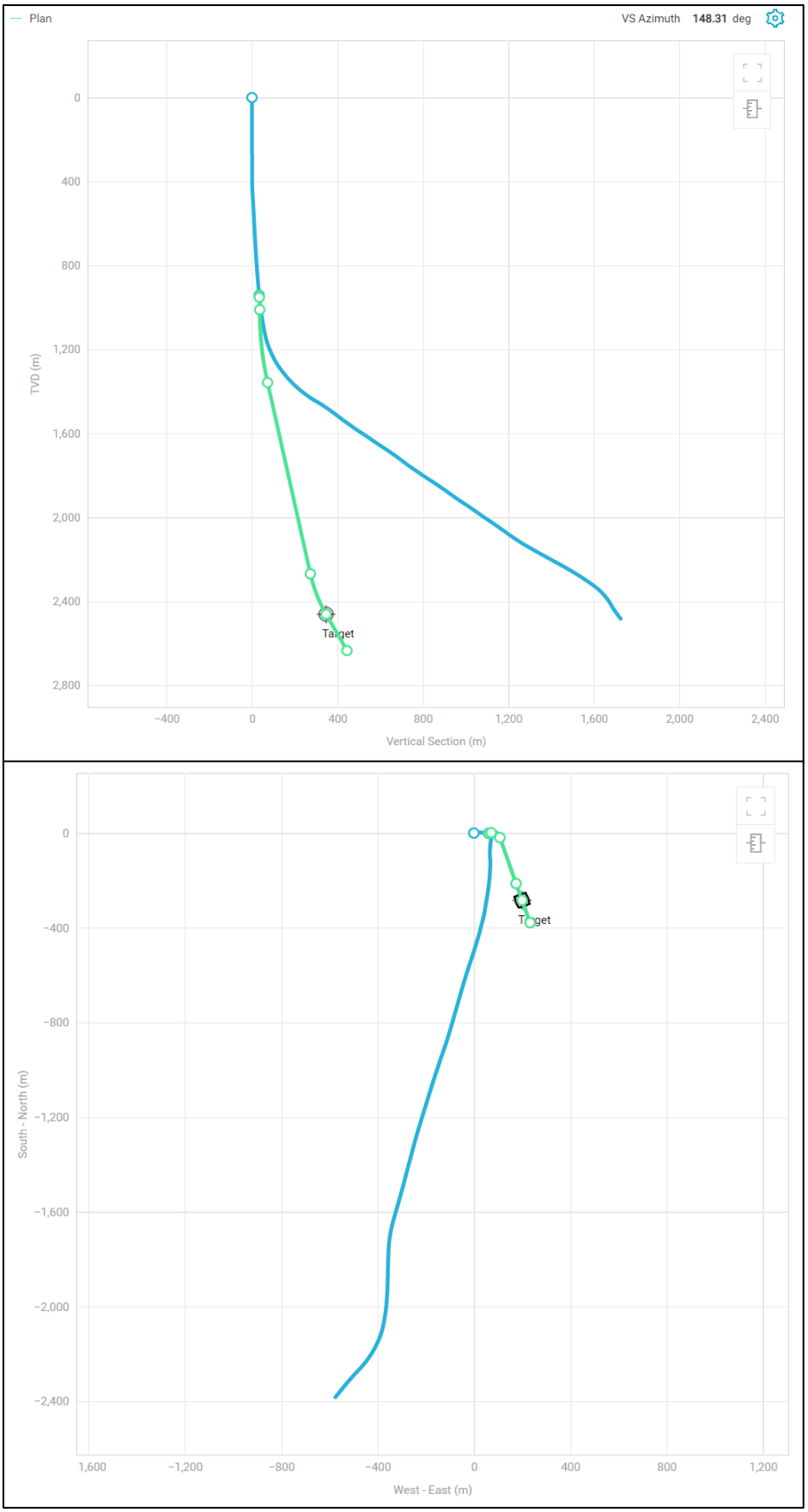

Figure 3.1 - Trajectory of Loris-234.
Sidetrack - Green line. Existing wellbore - Blue line.

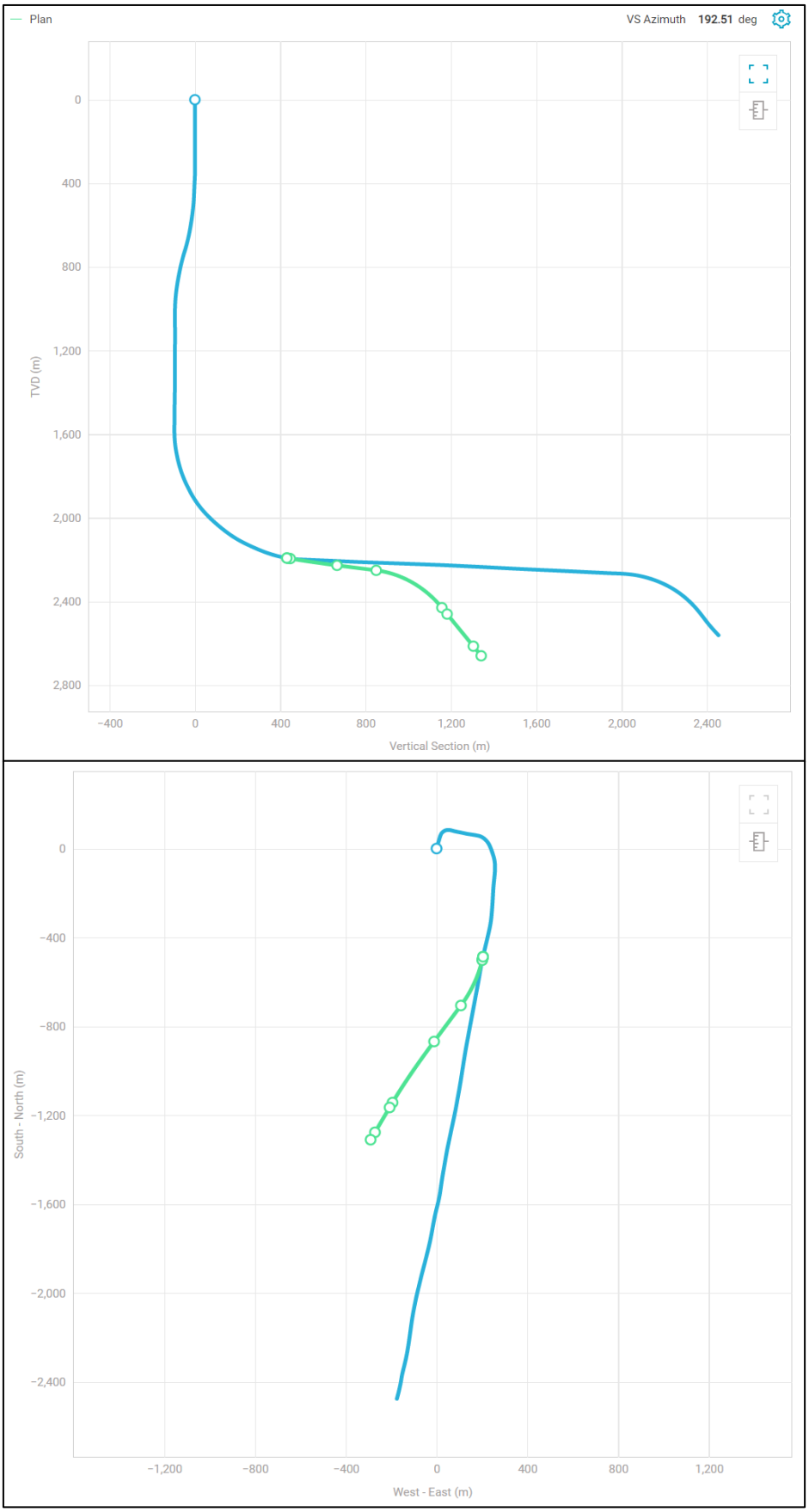

Figure 3.2 - Trajectory of Loris-345.
Sidetrack - Green line. Existing wellbore - Blue line.

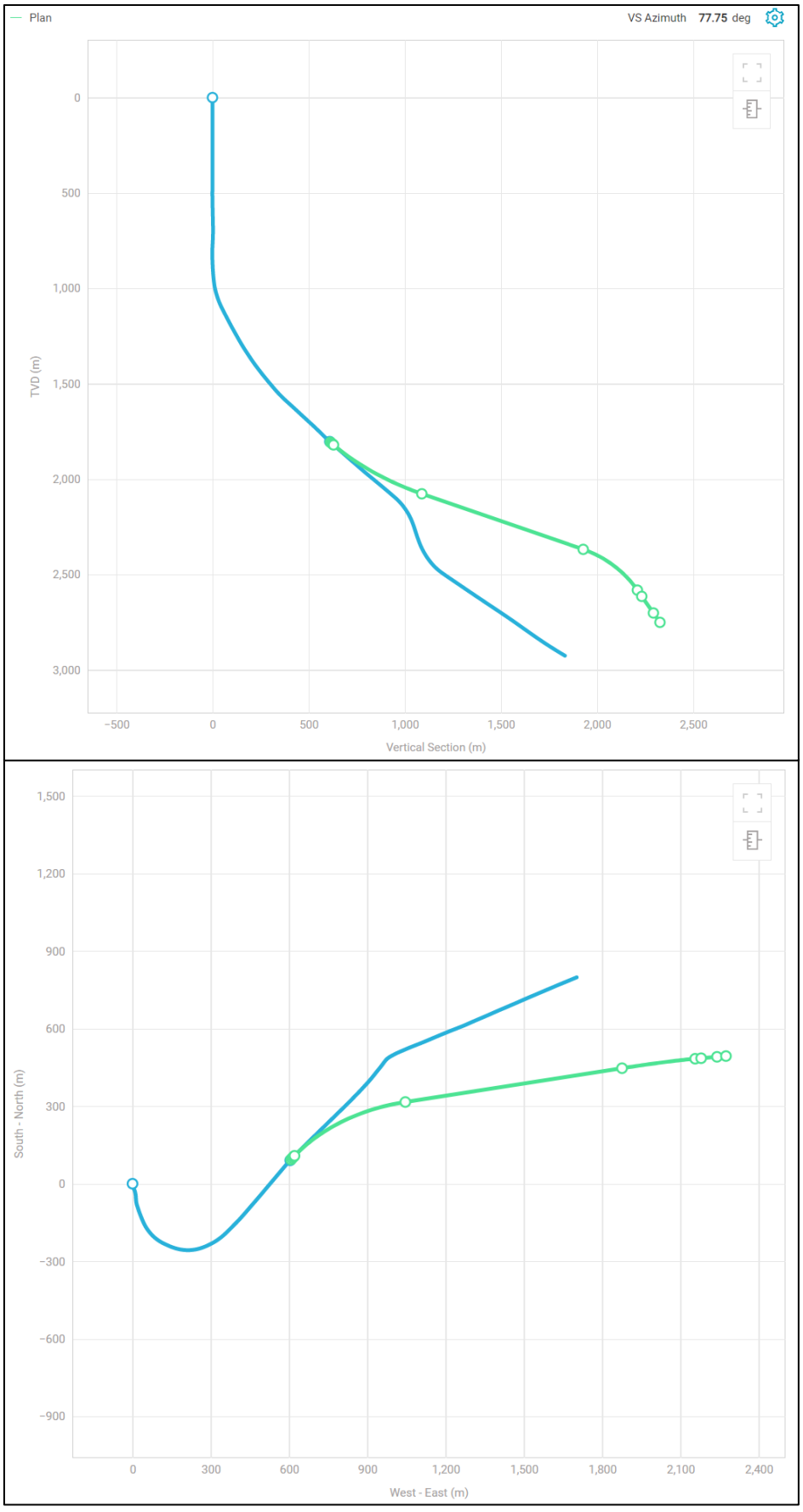

Figure 3.3- Trajectory of Loris-567.
Sidetrack - Green line. Existing wellbore - Blue line.

3.3 Well setup in DrillPlan

Different input data is required to perform hydraulic analysis in DrillPlan. The upcoming figures below in chapter *3.3 Well setup in DrillPlan*, shows some examples of what kind of information DrillPlan requires before hydraulic analysis can be implemented.

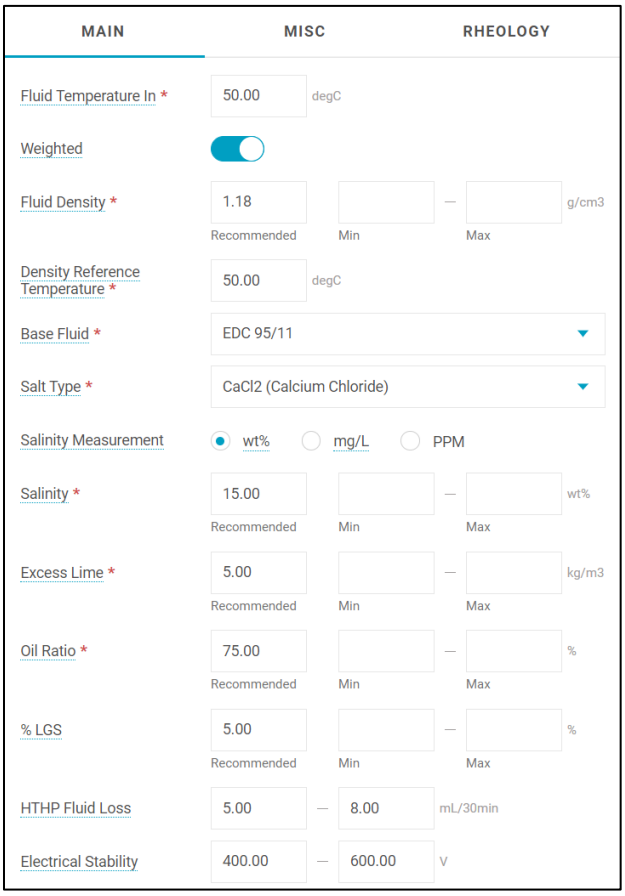

Figure 3.4 - Main characteristics necessary for hydraulic analysis in DrillPlan.

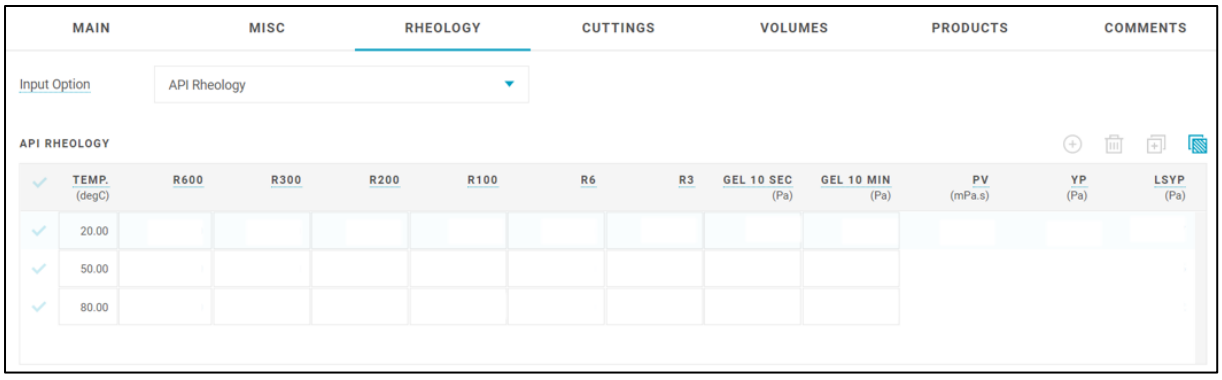

Figure 3.5 - Format of necessary rheological input data that must be entered.

Figure 3.6 - Rheological data format for high temperature, high pressure rheology can be used if necessary.

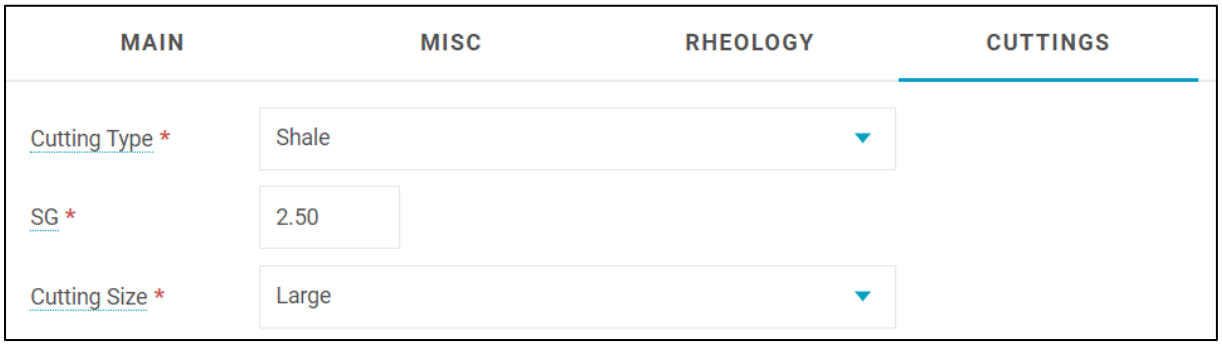

Figure 3.7 - Cutting type, cutting density and cutting size must be selected and entered.

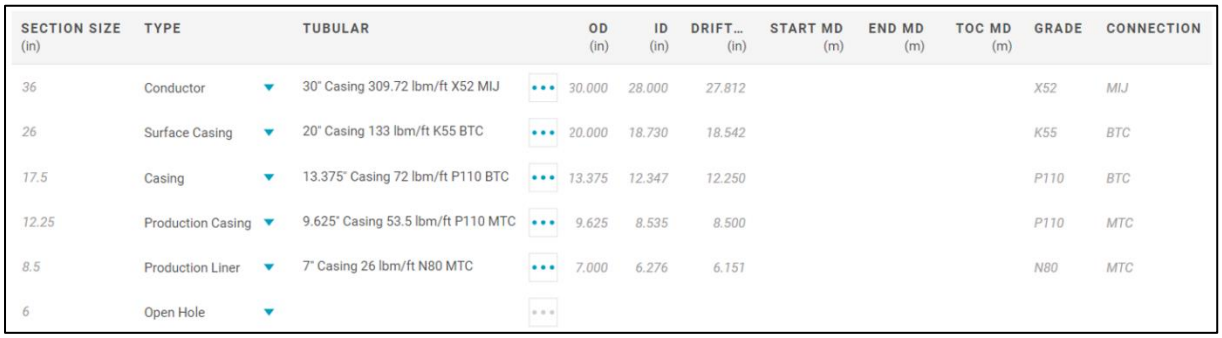

Figure 3.8 - Casing selection and casing related data must be entered to run hydraulic analysis.

3.4 Simulations with planning drilling parameters

Simulations with planning parameters were run with generic parameters based on the section size. These parameters are the same as used during well planning. Such a method is applied in well planning to save time and to provide comparable results when evaluating different well designs. DrillPlan has functionality to correct circulating temperatures based on offset well analysis. During initial planning this temperature correction is normally not applied, but it is applied during detailed engineering when a well design concept is selected. For this thesis, temperature correction for planning temperature is not applied.

3.5 Simulations with actual drilling parameters

To identify the actual drilling parameters used, real-time data containing measured drilling parameters from surface equipment (like mud pumps, top drive and draw works) and downhole equipment (measurement while drilling (MWD) tools) was downloaded from Schlumberger's InterACT system. The data was then plotted, and a parameter interval table was prepared for each different parameter. *Figure 3.9* shows an example of the flow rate parameter for one of the drilled sections.

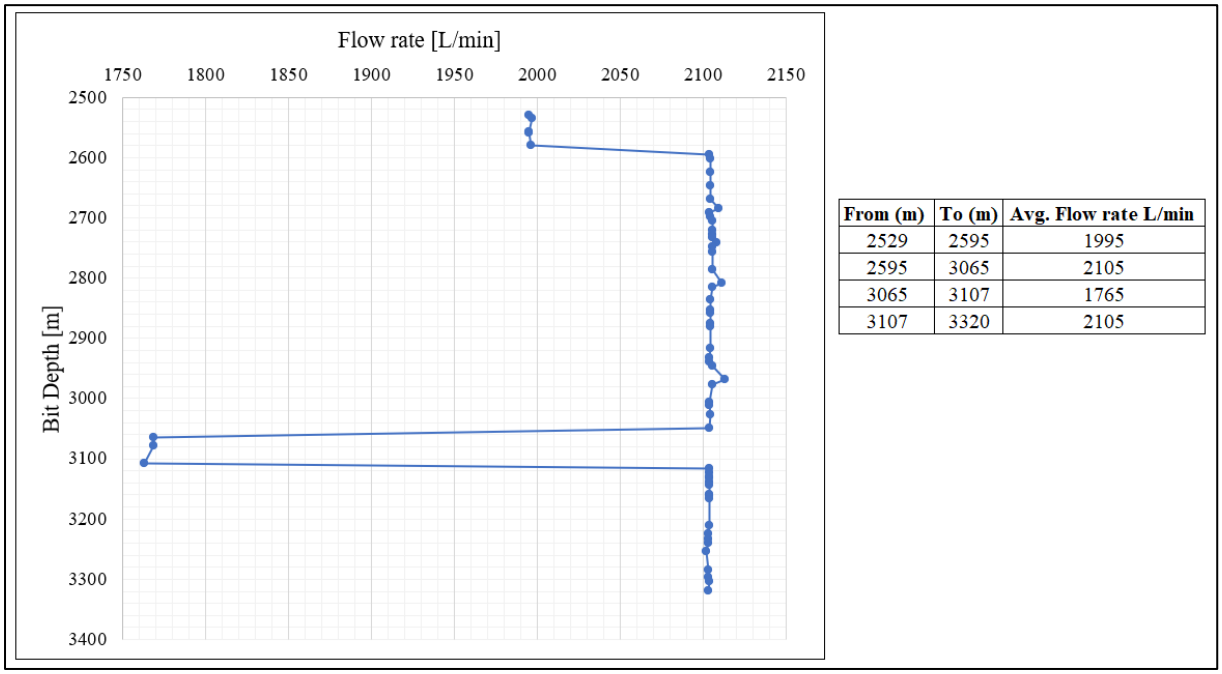

From (m)	To (m)	Avg. Flow rate L/min
2529	2595	1995
2595	3065	2105
3065	3107	1765
3107	3320	2105

Figure 3.9 - Parameter interval table showing average flow rates for different bit depth intervals.

Based on the parameter interval table, DrillPlan was used to perform sensitivity analysis to obtain the simulated ECDs and downhole temperature for the actual drilling parameters for the specific bit depths.

Sensitivity analysis functionality in DrillPlan allows the user to specify a depth interval and sample rate. For short well sections, 30 $meters$ depth intervals were used, while 60 $meters$ to 120 $meters$ depth intervals were used for longer drilled sections to be able to process the data sets. The sample rate was always set to split the range between the minimum and maximum parameter values in five.

The sensitivity analysis is multi-depth and runs all combinations of drilling parameters. As an example, for a section from 3300 $meter$ to 3570 $meter$ the sensitivity analysis will calculate hydraulics, torque and drag every 30-$meter$ increment, and the resulting effects all the way up to surface. *Figure 3.10* illustrates a simplified example of how sensitivity analysis is performed in DrillPlan. Red- and purple lines illustrate different results based on branching. A more complex example can be seen in *Figure 3.11*. This figure illustrates how DrillPlan presents the sensitivity analysis flow chart.

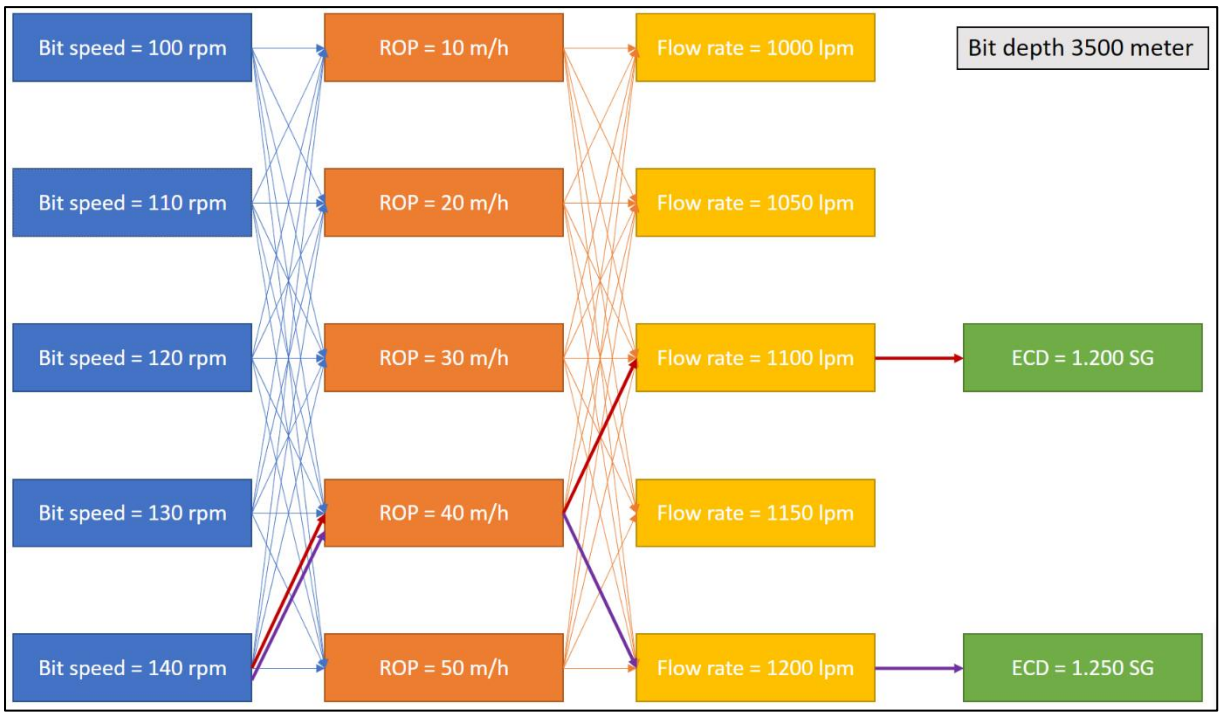

Figure 3.10 - Sensitivity analysis flow chart - a simplified example.

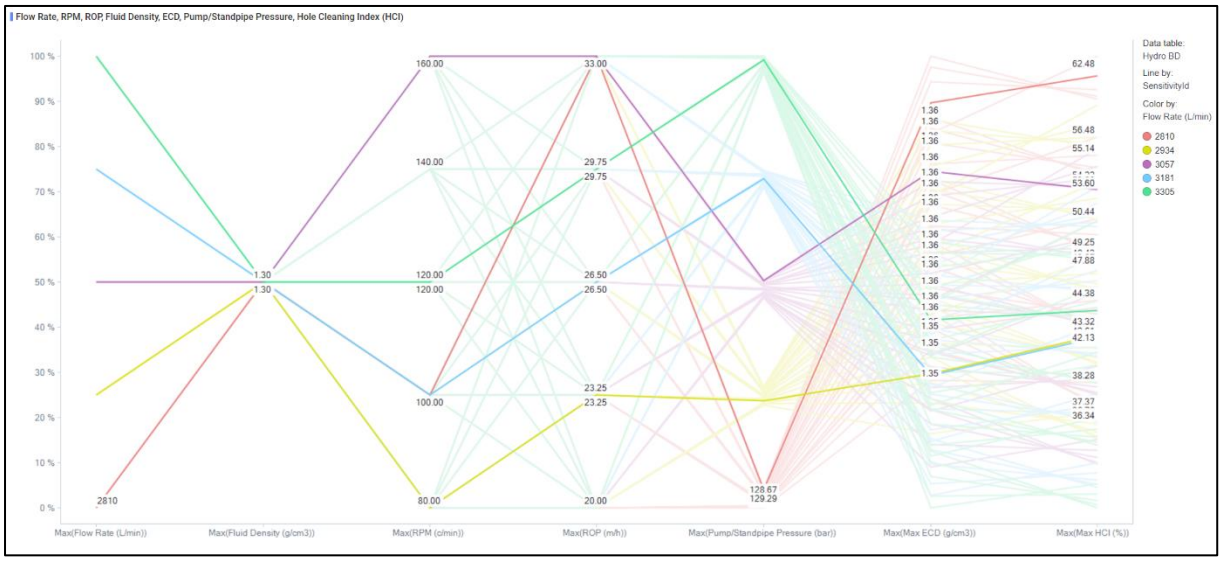

Figure 3.11 - Sensitivity analysis flow chart. An example of how it looks like in DrillPlan. By following the highlighted blue line, it is possible to see that a flow rate of 3181 L/min, a fluid density of 1.30 g/cm^3, a bit rotation of 100 RPM, a rate of penetration of 26.5 m/h, gives maximum equivalent circulating density (ECD) value 1.35 g/cm^3. The other highlighted colors show examples of different paths to calculated ECD values, while the non-highlighted colors illustrate all other possible paths to calculated ECD values.

As an example, the bit depth column in *Table 3.1* contains the bit depths at which a simulation has been performed in DrillPlan. Based on this, the drilling parameters are mapped from the parameter interval table. As the actual drilling parameters can vary significantly, the parameters had to be mapped to the closest match available from the multi-depth simulation. This makes it possible to find the ECD and annulus temperature for a specific bit depth, with given drilling parameters at that depth.

Table 3.1 - Example that shows basis of simulated ECD- and annulus temperature with actual parameters.

Bit depth (m)	Bit rotation (RPM)	ROP (m/h)	Flow rate (L/min)	ECD w/ cuttings (SG)	ECD w/o cuttings (SG)	Annulus temperature (°C)
2561	127	29	2020	1.725	1.718	60.2
2621	127	29	2105	1.711	1.704	72.9
2681	127	23	2105	1.724	1.719	67.1
2741	143	23	2105	1.727	1.722	68.3
2801	143	23	2105	1.717	1.711	75.6
2861	143	41	2105	1.721	1.712	77.4
2921	143	41	2105	1.722	1.712	78.7
2981	143	17	2105	1.717	1.713	80.2
3041	143	35	2105	1.722	1.714	81.1
3101	143	23	1765	1.716	1.710	79.1
3161	143	35	2105	1.722	1.714	82.9
3221	143	41	2105	1.723	1.714	83.9
3281	143	35	2105	1.721	1.713	85.2
3330	143	35	2105	1.721	1.712	85.7

4. Results

The resulting figures and tables created from the simulations of the three wells and associated sections, will be shown in the upcoming subchapters.

4.1.1 Loris-234_13.5in

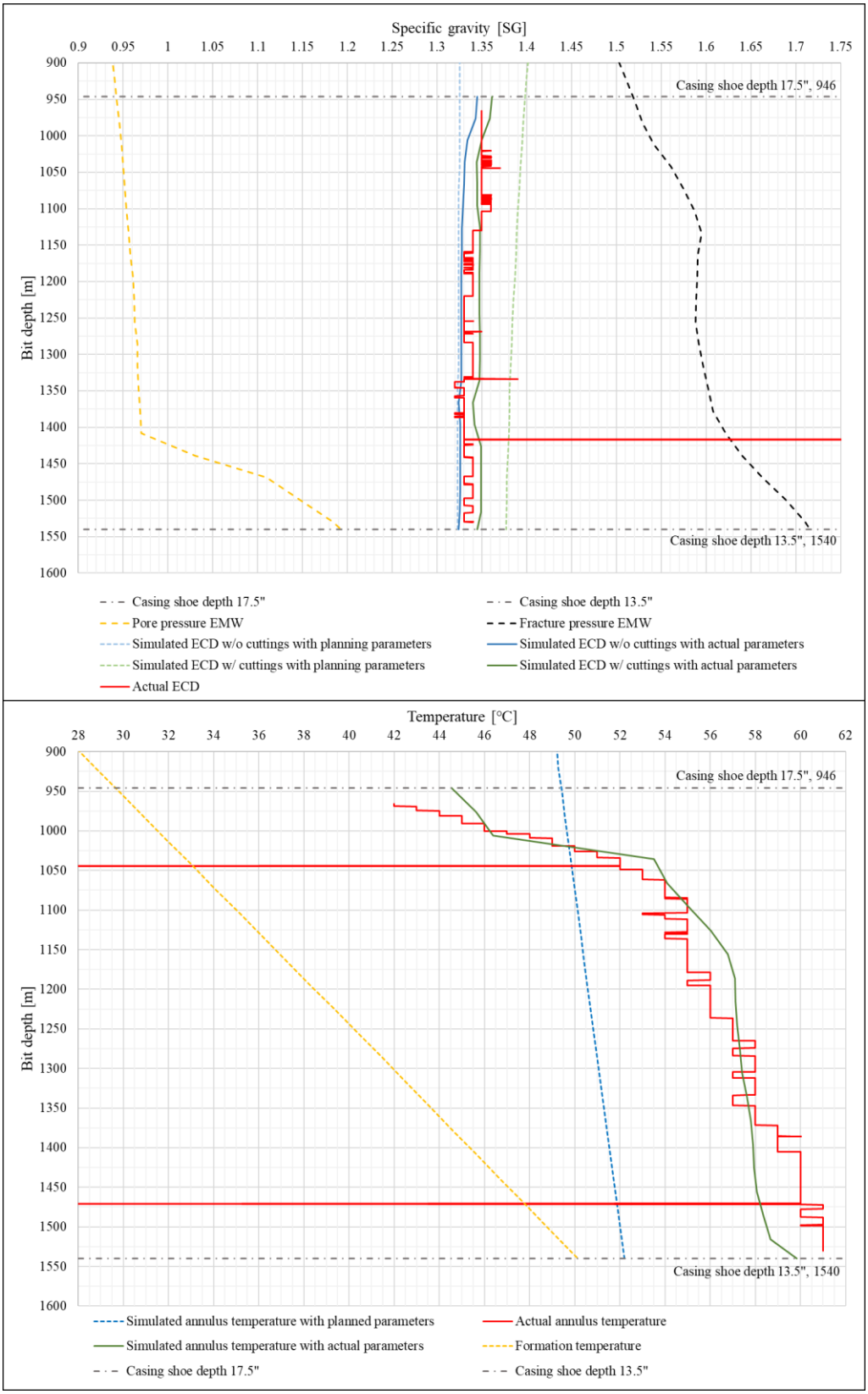

Figure 4.1 - Loris-234_13.5in.
Bit depth vs Specific gravity & Bit depth vs Temperature.
Interval [946 - 1540] meter.

Table 4.1 - Deviations Loris-234_13.5in:
Simulated ECD with actual parameters vs Actual ECD averaged
± 5 meter around simulated bit depth.

Bit depth (m)	ECD w/ cuttings (SG)	ECD w/o cuttings (SG)	Actual ECD (SG)	Delta w/ cuttings (SG)	Delta w/o cuttings (SG)
946	1.361	1.345	No data	No data	No data
976	1.359	1.343	1.350	0.009	-0.007
1006	1.350	1.334	1.350	0.000	-0.016
1036	1.344	1.331	1.353	-0.009	-0.022
1066	1.345	1.330	1.350	-0.005	-0.020
1096	1.345	1.329	1.358	-0.013	-0.029
1126	1.348	1.328	1.349	-0.001	-0.021
1156	1.348	1.328	1.339	0.009	-0.011
1186	1.347	1.327	1.336	0.011	-0.009
1216	1.347	1.327	1.339	0.008	-0.012
1246	1.347	1.327	1.330	0.017	-0.003
1276	1.348	1.327	1.330	0.018	-0.003
1306	1.348	1.327	1.340	0.008	-0.013
1336	1.347	1.327	1.329	0.018	-0.002
1366	1.340	1.324	1.330	0.010	-0.006
1396	1.342	1.326	1.330	0.012	-0.004
1426	1.349	1.326	1.331	0.018	-0.005
1456	1.349	1.326	1.340	0.009	-0.014
1486	1.349	1.326	1.340	0.009	-0.014
1516	1.349	1.325	1.336	0.013	-0.011
1540	1.345	1.324	No data	No data	No data
Min value (SG)				-0.013	-0.029
Average value (SG)				0.007	-0.012
Max value (SG)				0.018	-0.002

4.1.2 Loris-234_12.25in

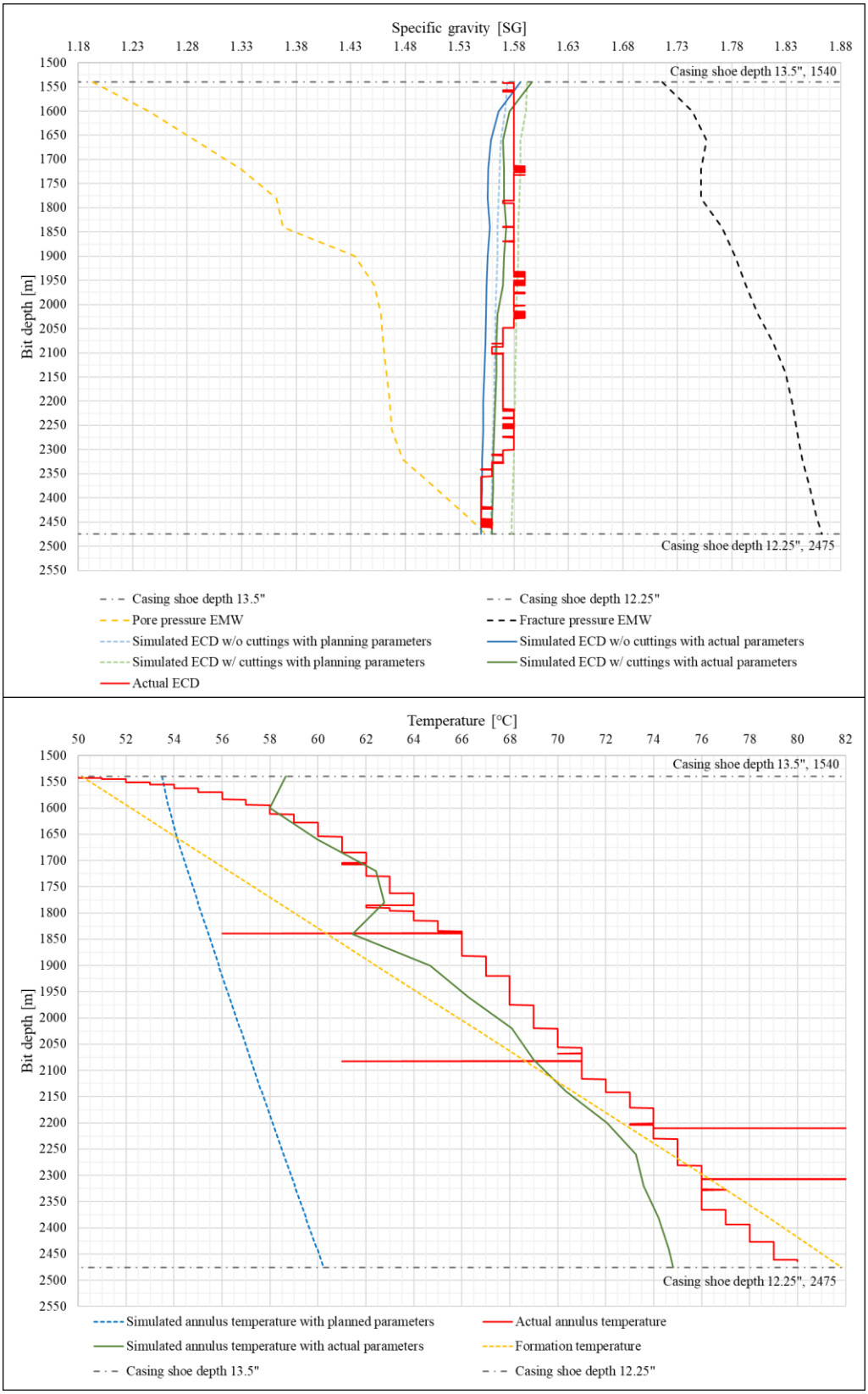

Figure 4.2 - Loris-234_12.25in.
Bit depth vs Specific gravity & Bit depth vs Temperature.
Interval [1540 - 2475] meter.

Table 4.2 - Deviations Loris-234_12.25in:
Simulated ECD with actual parameters vs Actual ECD averaged
± 5 meter around simulated bit depth.

Bit depth (m)	ECD w/ cuttings (SG)	ECD w/o cuttings (SG)	Actual ECD (SG)	Delta w/ cuttings (SG)	Delta w/o cuttings (SG)
1540	1.597	1.586	1.576	0.021	0.010
1600	1.576	1.566	1.580	-0.004	-0.014
1660	1.570	1.559	1.580	-0.010	-0.021
1720	1.571	1.557	1.585	-0.014	-0.028
1780	1.571	1.556	1.580	-0.009	-0.024
1840	1.573	1.558	1.579	-0.007	-0.021
1900	1.571	1.556	1.580	-0.009	-0.024
1960	1.570	1.555	1.581	-0.011	-0.026
2020	1.565	1.554	1.588	-0.023	-0.033
2080	1.564	1.554	1.570	-0.006	-0.016
2140	1.564	1.553	1.570	-0.006	-0.017
2200	1.563	1.552	1.570	-0.007	-0.018
2260	1.562	1.552	1.579	-0.017	-0.027
2320	1.561	1.551	1.570	-0.009	-0.019
2380	1.561	1.551	1.550	0.011	0.001
2440	1.560	1.550	1.550	0.010	0.000
2475	1.560	1.550	No data	No data	No data
Min value (SG)				-0.023	-0.033
Average value (SG)				-0.006	-0.017
Max value (SG)				0.021	0.010

4.1.3 Figure comparison of Bit depth vs Specific gravity for Loris-234 sections

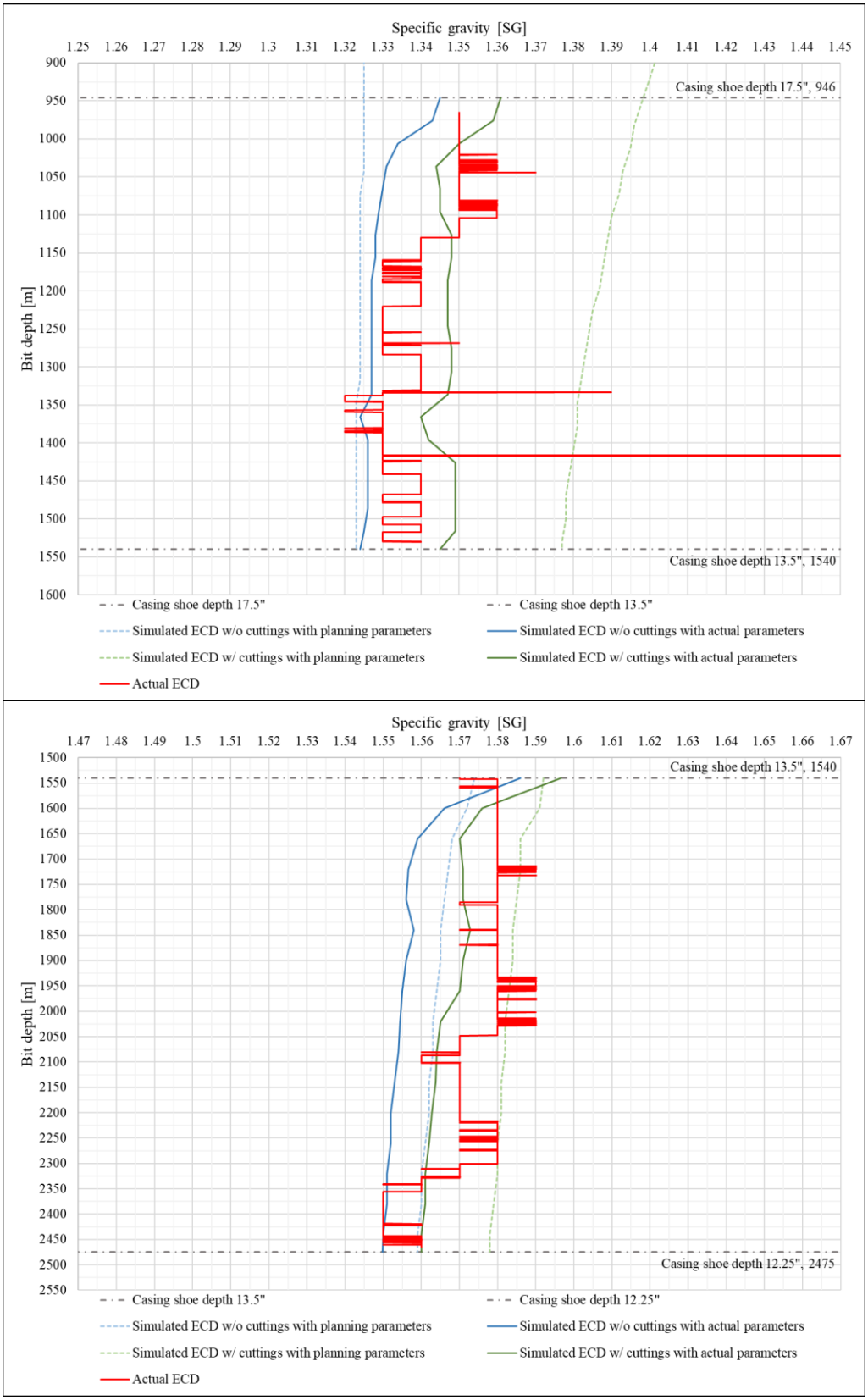

Figure 4.3 - Comparison of Loris-234 sections.
13.5in (top) and 12.25in (bottom).
X-axis: Interval with 0.2 SG as difference between max- and min x-value.

4.2.1 Loris-345_8.5in

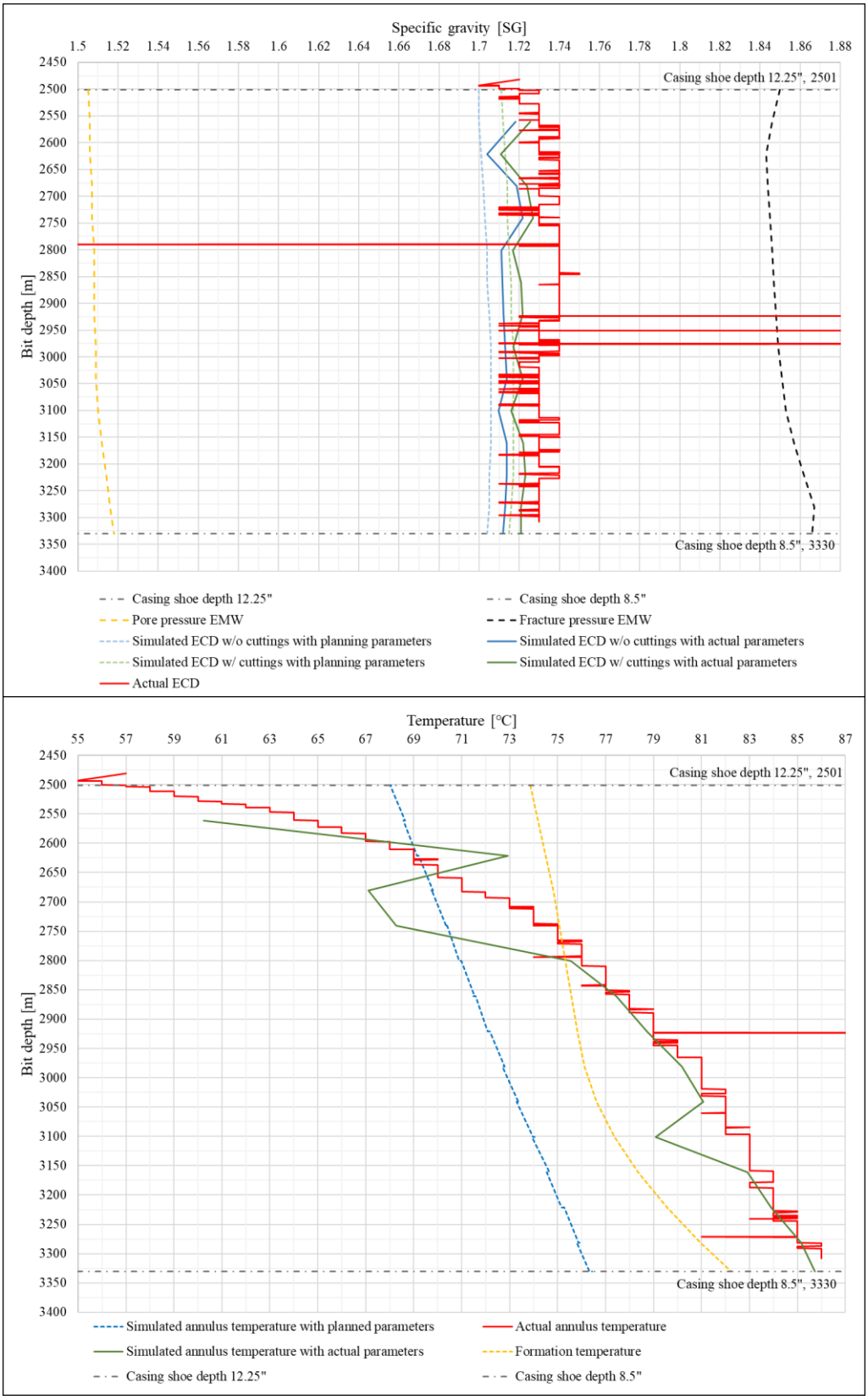

Figure 4.4 - Loris-345_8.5in.
Bit depth vs Specific gravity & Bit depth vs Temperature.
Interval [2501 - 3330] meter.

Table 4.3 - Deviations Loris-345_8.5:
Simulated ECD with actual parameters vs Actual ECD averaged
± 5 meter around simulated bit depth.

Bit depth (m)	ECD w/ cuttings (SG)	ECD w/o cuttings (SG)	Actual ECD (SG)	Delta w/ cuttings (SG)	Delta w/o cuttings (SG)
2561	1.725	1.718	1.730	-0.004	-0.012
2621	1.711	1.704	1.737	-0.026	-0.033
2681	1.724	1.719	1.735	-0.011	-0.016
2741	1.727	1.722	1.731	-0.004	-0.009
2801	1.717	1.711	1.740	-0.023	-0.029
2861	1.721	1.712	1.740	-0.019	-0.028
2921	1.722	1.712	1.736	-0.014	-0.024
2981	1.717	1.713	1.738	-0.021	-0.025
3041	1.722	1.714	1.728	-0.006	-0.014
3101	1.716	1.710	1.730	-0.014	-0.020
3161	1.722	1.714	1.730	-0.008	-0.016
3221	1.723	1.714	1.734	-0.011	-0.020
3281	1.721	1.713	1.730	-0.009	-0.017
3330	1.721	1.712	No data	No data	No data
Min value (SG)				-0.026	-0.033
Average value (SG)				-0.013	-0.020
Max value (SG)				-0.004	-0.009

4.2.1 Loris-345_6in

Figure 4.5 - Loris-345_6in.
Bit depth vs Specific gravity & Bit depth vs Temperature.
Interval [3330 - 3570] meter.

Table 4.4- Deviations Loris-345_6in:
Simulated ECD with actual parameters vs Actual ECD averaged
$\pm$ 5 meter around simulated bit depth.

Bit depth (m)	ECD w/ cuttings (SG)	ECD w/o cuttings (SG)	Actual ECD (SG)	Delta w/ cuttings (SG)	Delta w/o cuttings (SG)
3330	1.259	1.246	1.280	-0.021	-0.034
3360	1.261	1.248	1.280	-0.019	-0.032
3390	1.264	1.249	1.279	-0.015	-0.030
3420	1.269	1.251	1.280	-0.011	-0.029
3450	1.271	1.255	1.280	-0.009	-0.025
3480	1.272	1.256	1.290	-0.018	-0.034
3510	1.273	1.256	1.292	-0.019	-0.036
3540	1.269	1.257	1.300	-0.031	-0.043
3570	1.270	1.257	1.308	-0.038	-0.051
Min value (SG)				-0.038	-0.051
Average value (SG)				-0.020	-0.035
Max value (SG)				-0.009	-0.025

4.2.3 Figure comparison of Bit depth vs Specific gravity for Loris-345 sections

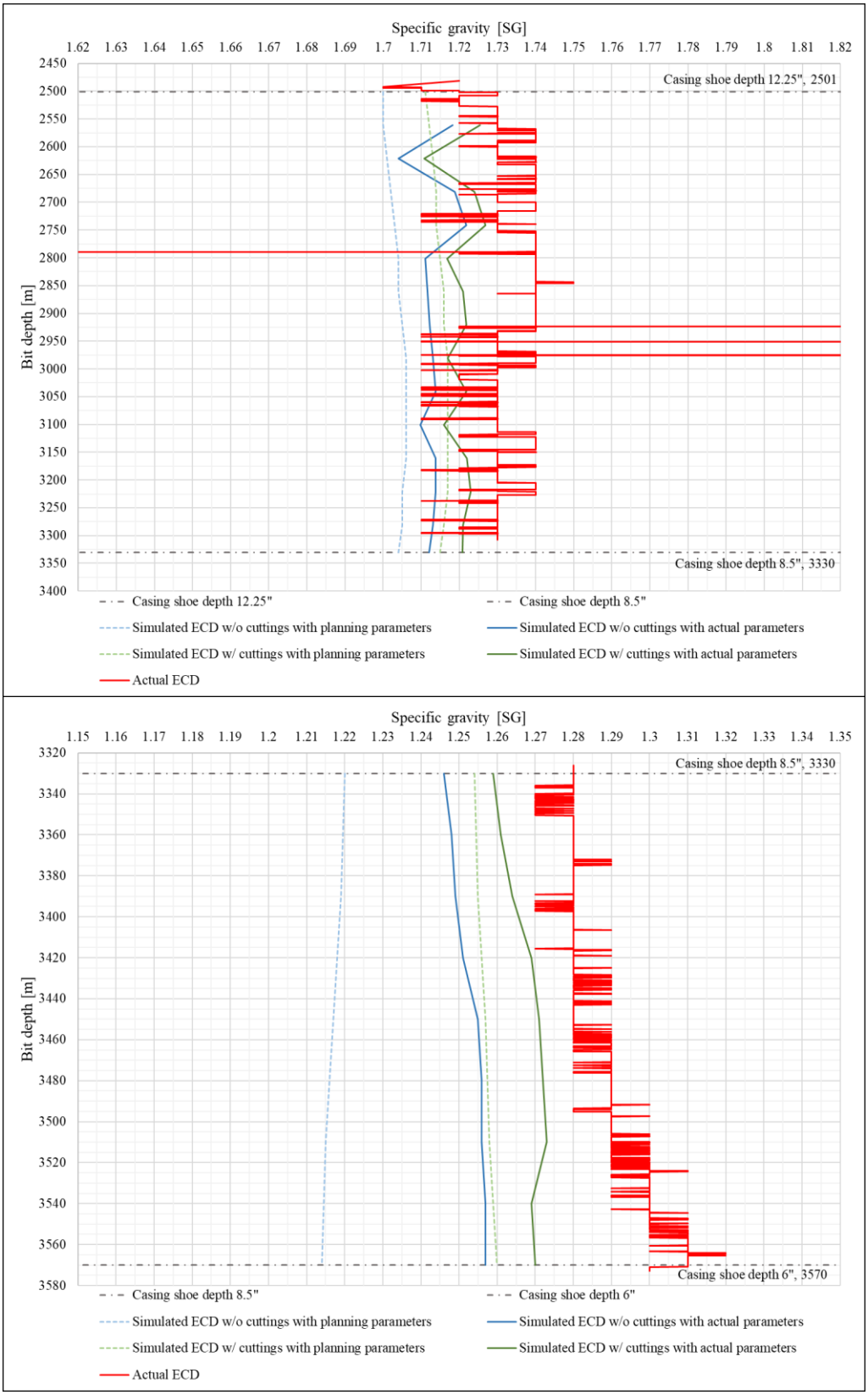

Figure 4.6 - Comparison of Loris-345 sections.
8.5in (top) and 6in (bottom).
X-axis: Interval with 0.2 SG as difference between max- and min x-value.

4.3.1 Loris-567_8.5in

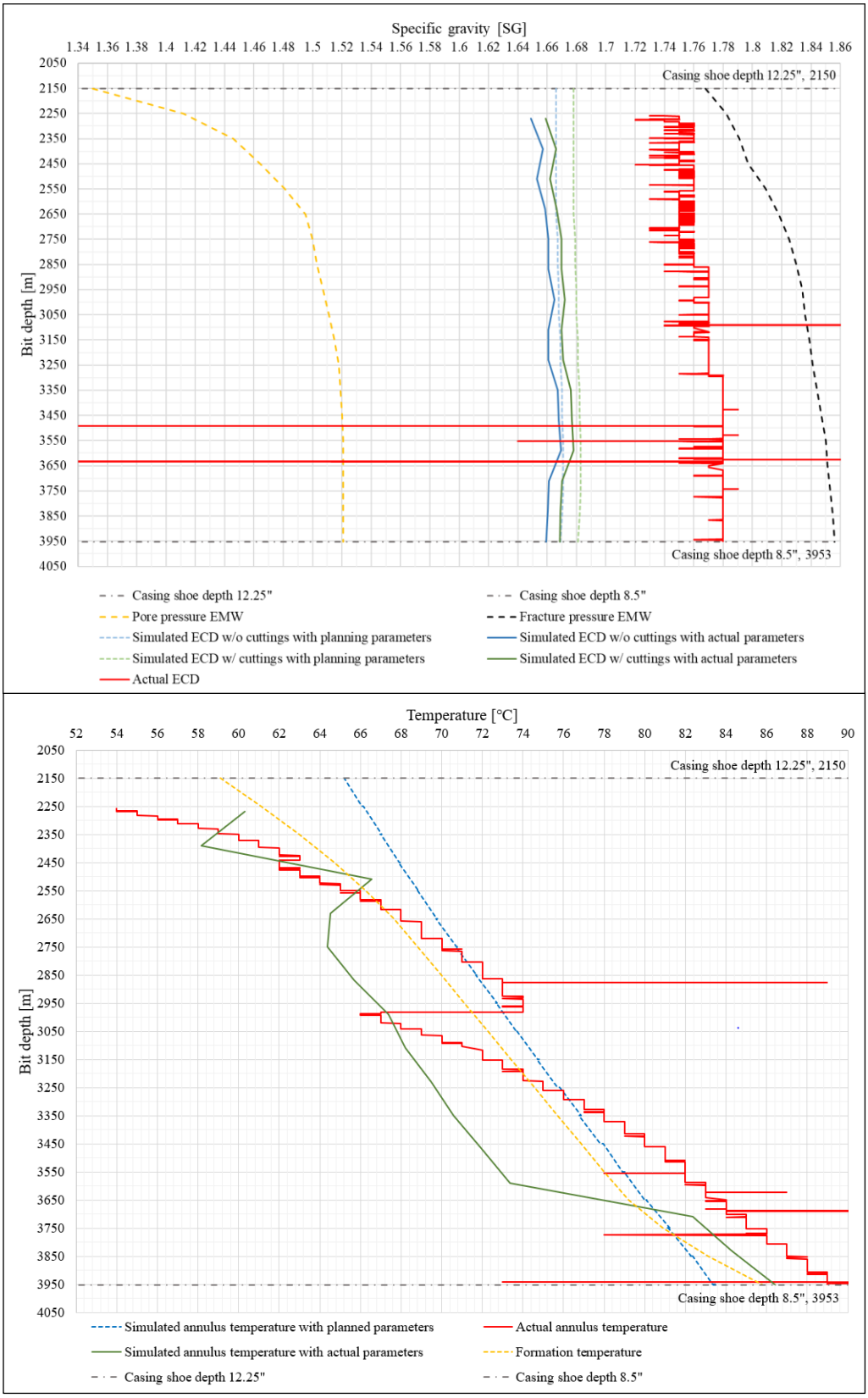

Figure 4.7 - Loris-567_8.5in.
Bit depth vs Specific gravity & Bit depth vs Temperature.
Interval [2150 - 3953] meter.

Table 4.5 - Deviations Loris-567_8.5in:
Simulated ECD with actual parameters vs Actual ECD averaged
± 5 meter around simulated bit depth.

Bit depth (m)	ECD w/ cuttings (SG)	ECD w/o cuttings (SG)	Actual ECD (SG)	Delta w/ cuttings (SG)	Delta w/o cuttings (SG)
2270	1.659	1.649	1.745	-0.086	-0.096
2390	1.666	1.657	1.748	-0.082	-0.091
2510	1.662	1.653	1.758	-0.096	-0.105
2630	1.667	1.659	1.753	-0.086	-0.094
2750	1.670	1.661	1.756	-0.086	-0.095
2870	1.670	1.661	1.770	-0.100	-0.109
2990	1.672	1.665	1.759	-0.087	-0.094
3110	1.670	1.661	No data	No data	No data
3230	1.671	1.661	1.770	-0.099	-0.109
3350	1.676	1.667	1.780	-0.104	-0.113
3470	1.677	1.668	1.780	-0.103	-0.112
3590	1.678	1.669	1.780	-0.102	-0.111
3710	1.670	1.661	1.780	-0.110	-0.119
3830	1.669	1.661	1.780	-0.111	-0.119
3950	1.669	1.659	1.780	-0.111	-0.121
3953	1.669	1.659	1.780	-0.111	-0.121
Min value (SG)				-0.111	-0.121
Average value (SG)				-0.098	-0.107
Max value (SG)				-0.082	-0.091

4.3.2 Loris-567_6in

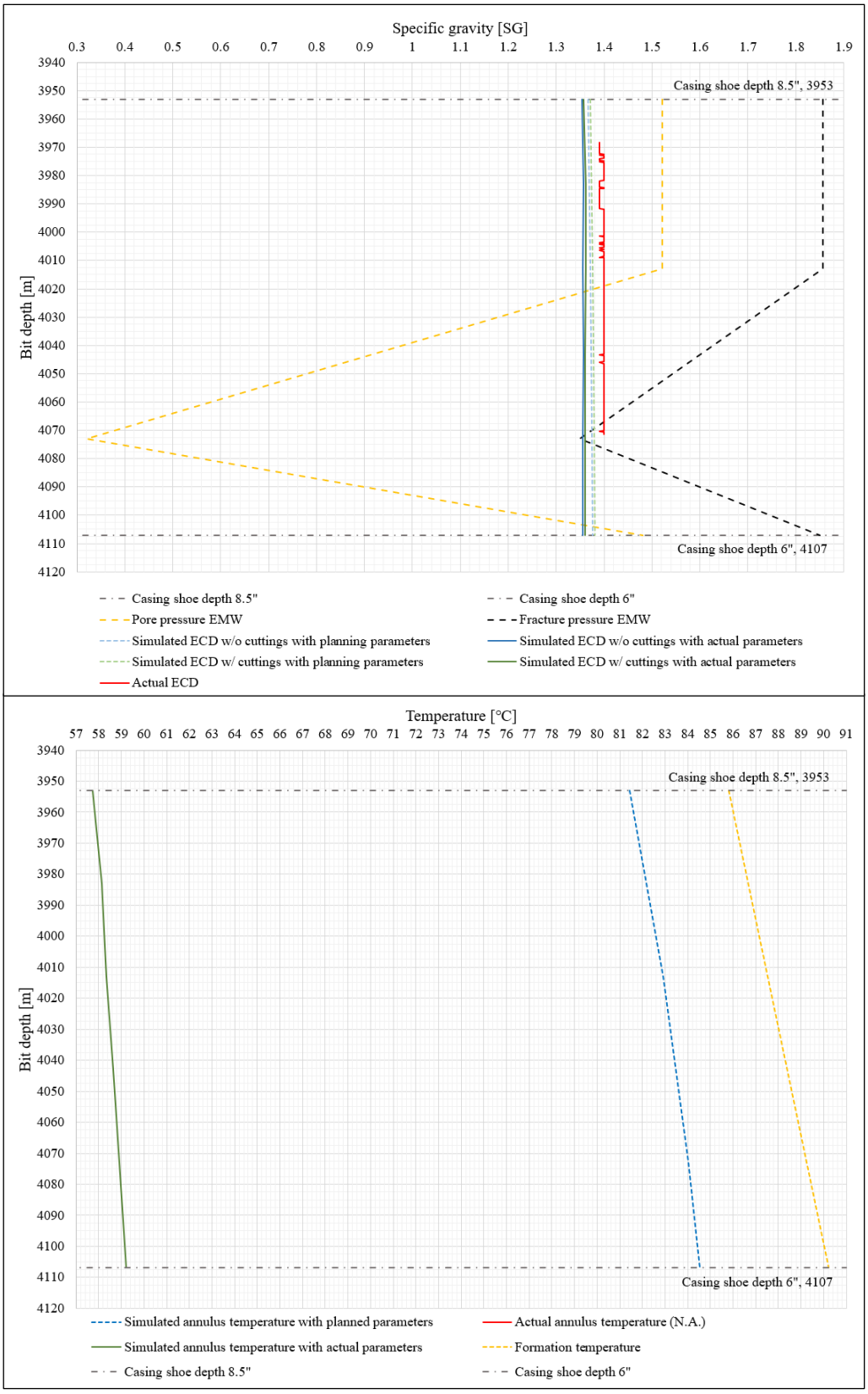

Figure 4.8 - Loris-567_6in.
Bit depth vs Specific gravity & Bit depth vs Temperature.
Interval [3953 - 4107] meter. Actual annulus temperature not available (N.A.).

Table 4.6 - Deviations Loris-567_6in:
Simulated ECD with actual parameters vs Actual ECD averaged
$\pm$ 5 meter around simulated bit depth.

Bit depth (m)	ECD w/ cuttings (SG)	ECD w/o cuttings (SG)	Actual ECD (SG)	Delta w/ cuttings (SG)	Delta w/o cuttings (SG)
3953	1.357	1.354	No data	No data	No data
3983	1.362	1.357	1.394	-0.032	-0.037
4013	1.362	1.356	1.400	-0.038	-0.044
4043	1.361	1.357	1.399	-0.038	-0.042
4073	1.361	1.355	1.399	-0.038	-0.044
4103	1.361	1.355	No data	No data	No data
Min value (SG)				-0.038	-0.044
Average value (SG)				-0.037	-0.042
Max value (SG)				-0.032	-0.037

4.3.3 Figure comparison of Bit depth vs Specific gravity for Loris-567 sections

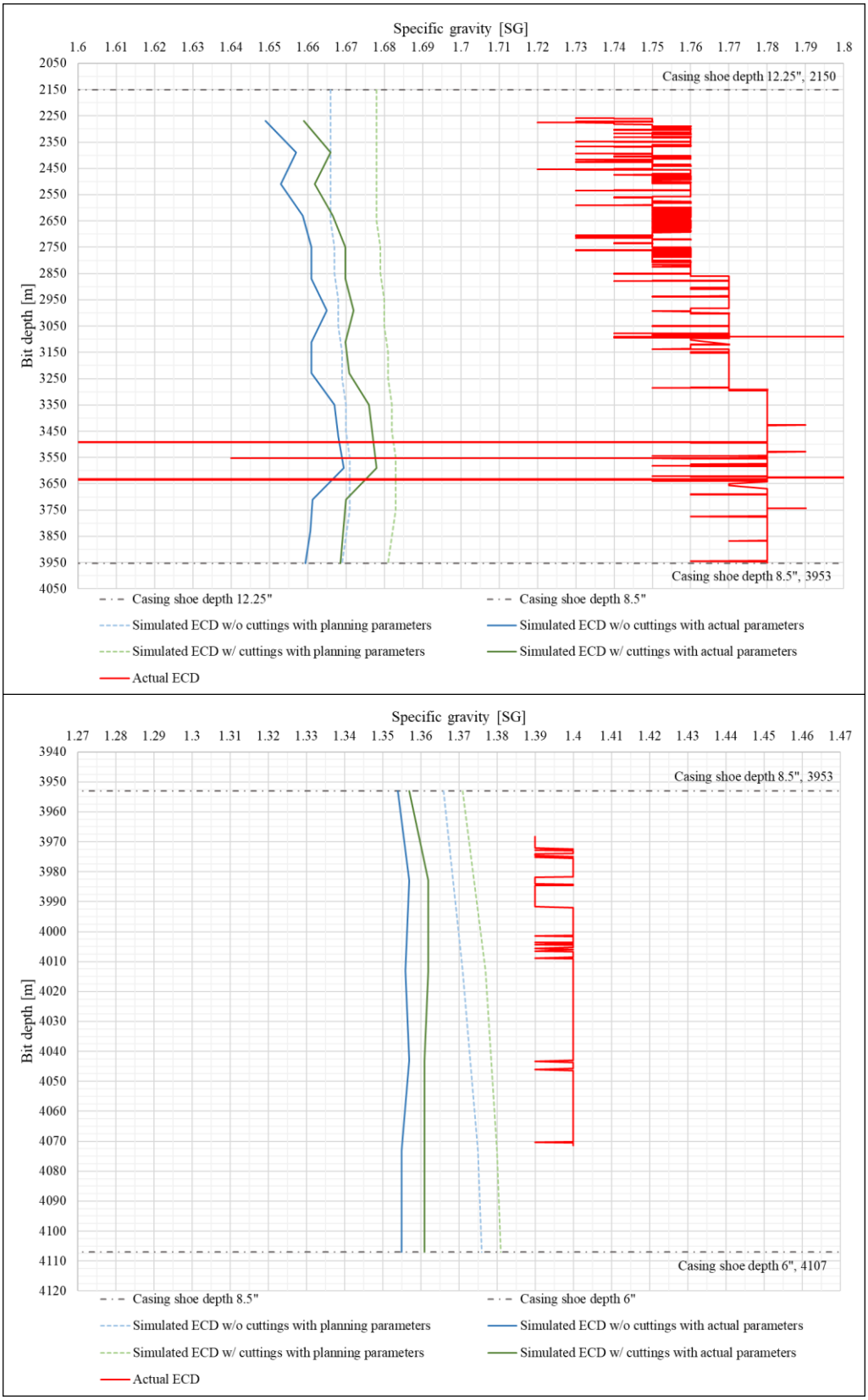

Figure 4.9 - Comparison of Loris-567 sections.
8.5in (top) and 6in (bottom).
X-axis: Interval with 0.2 SG as difference between max- and min x-value.

5. Discussion

When it comes to the figures that shows bit depth vs specific gravity in chapter *4. Results*, the desired results are that the actual ECD (red solid line) lies somewhere between simulated ECD without cuttings using actual parameters (solid blue line) and simulated ECD with cuttings using actual parameters (solid green line). It is expected that actual ECD will be closest to the simulated ECD with cuttings using actual parameters. For the bit depth vs temperature plots, it is desired that simulated annulus temperature with actual parameters (solid green line) follows and are even to the actual annulus temperature (solid red line).

The large discrepancies, i.e., low- and high spikes, are bad data points and are due to transmission errors in equipment. These discrepancies have not been filtered out but note that these data spikes are not considered valid.

Formation temperature is obtained by applying the linear temperature gradient provided and is only included as a reference temperature. It is not expected to match any of the other temperature data. The simulated and actual numbers reflect state of a drilling where one has both cooling from circulation and heat generated by friction from the drill bit, as well as heat from drill string friction being imposed on the well. The data series with annulus temperature using planned parameters (dotted blue lines) does not have offset well temperature correction applied. This deviates from normal engineering practice during well planning, where temperature calibration is performed by looking at offset well data as part of the planning phase.

At the beginning of the drilling sections, the drilling fluid is cold i.e., at surface temperature, resulting in higher ECDs. During drilling and circulation, the drilling fluid temperature increases, which further leads to lower ECD due to lower viscosity. A good example can be seen in *Figure 4.3*, which also is consistent with the theory, *2.3.2 Pressure- and temperature effects on drilling fluids density*.

The term fluid in temperature is here referred to as the drilling fluid temperature when the drilling fluid enters the drill string. Based on a historical basis for the average surface temperature in the mud pits, this has been chosen to be 45℃. Furthermore, one can observe in the temperature plots in chapter *4. Results*, that simulated annulus temperature with actual parameters differs somewhat from the actual annulus temperature measured in the beginning of the drilled sections. The reason for these discrepancies is that DrillPlan does not take into account the lower temperature at the beginning of the drilling run, but it assumes that the circulating temperature of the drilling fluid has reached thermal equilibrium when drilling.

5.1.1 Discussion - Loris-234_13.5in

Figure 4.1 illustrates that all the ECD-values are safely present in the middle of the pore- and fracture pressure window. The highest specific gravity values at different bit depths turns out to be for the simulated ECD with cuttings using planning parameters, while the lowest specific gravity values at different bit depths is for the simulated ECD without cuttings using planning parameters. Actual ECD (red solid line) is mostly located between simulated ECD without cuttings using actual parameters (blue solid line) and simulated ECD with cuttings using actual parameters (green solid line), but there are exceptions. *Table 4.1* shows that the highest delta (i.e., ECD simulation minus actual ECD) with cuttings deviation is 0.018 SG, at e.g., 1426-$meter$ bit depth. An average positive delta with cuttings value of 0.007 SG and an average delta without cuttings value of -0.012 SG indicates that actual ECD is largely located in between simulated ECD with and without cuttings, but somewhat closer to the simulation with cuttings. The simulated annulus temperature with actual parameters follows the actual annulus temperature quite well.

5.1.2 Discussion - Loris-234_12.25in

When it comes to *Figure 4.2* and the 12.25-$inch$ section, the ECD-values are close to the pore pressure for the deepest bit depths, since the pore pressure increases with depth, while ECD-values stays approximately the same. Simulated ECD-values with planned parameters are evenly higher than the simulated ECD-values with actual parameters, i.e., dotted blue line to the right of solid blue line and dotted green line to the right of solid green line. The simulated ECD with and without cuttings using actual parameters are mostly below the actual ECD line. This is also reflected in *Table 4.2*, which shows negative average delta values both for the simulations with and without cuttings. Average delta value with cuttings was -0.006 SG, while average delta value without cuttings was -0.017 SG. A maximum deviation of -0.023 SG can be seen for delta with cuttings, and it occurred at 2020-$meter$ bit depth. Simulated annulus temperature with actual parameters deviates from the actual annulus temperature in the very beginning- and from 1800-$meter$ bit depth to end depth. From 1600-$meter$ bit depth to 1800-$meter$ bit depth, the temperatures correlate nicely.

5.2.1 Discussion - Loris-345_8.5in

For the Loris-345_8.5in section, *Figure 4.4* shows that all ECD-values are approximately in the center of the pore- and fracture pressure window. Simulated ECD without cuttings using planning parameters have the lowest ECD-values through the entire section. Simulations with actual parameters are below the actual ECD measured. This is also confirmed in *Table 4.3* with only negative min- and max values, and by negative average delta values of -0.013 SG with cuttings, and -0.020 SG without cuttings. The highest delta value with cuttings is -0.026 SG and it can be seen in the delta with cuttings column, at a bit depth of 2621-$meter$. Simulated annulus temperature with actual parameters correlates and fits decent with actual annulus temperature, although some larger divergent discrepancies can be seen at some bit depths.

5.2.2 Discussion - Loris-345_6in

Figure 4.5 illustrates that the ECD-values are below pore pressure in the beginning- and end of the drilled 6-$inch$ section due to entry into a depleted reservoir zone. The actual measured ECD have the highest ECD-values through the entire section. *Table 4.4* confirms that simulated ECD with and without cuttings using actual parameters deviates from actual ECD measured. The sharp increase in ECD during the last 60-$meter$ of the section indicates that there might be insufficient hole cleaning. All the negative delta values indicates that the simulated ECD-values using actual parameters always is lower than actual ECD. Average delta values with- and without cuttings are -0.020 SG and -0.035 SG, respectively. The largest delta with cuttings deviation can be seen at 3570-$meter$ bit depth, with a delta value of -0.038 SG. With the starting- and upper middle part temperatures as exception, simulated annulus temperature with actual parameters do follow the actual annulus temperature trend to a certain extent.

5.3.1 Discussion - Loris-567_8.5in

Loris-567_8.5in are plotted in *Figure 4.7* which shows a long section drilled. The actual measured ECD are much closer to the fracture pressure than the pore pressure. In addition, actual ECD-values measured are much larger than all the simulated ECD-values. Simulated ECD-value with planned parameters is slightly higher than simulated ECD-values with actual parameters. *Table 4.5* shows significant negative average delta values with- and without cuttings of, -0.098 SG and -0.107 SG, respectively. Maximum delta values are seen at the end of the sections, i.e., at the largest bit depths. The greatest delta with cuttings value is -0.111 SG. Simulated annulus temperature with actual parameters follows the actual annulus temperature quite poorly. At approximately 2970-$meter$ bit depth, a trip was performed to rearrange the drill pipe, and as a result the surface drilling fluid temperature cooled down. Effectively this restarted the temperature trend when the drilling recommenced. This was attempted to model in DrillPlan as one drilling run, but as the plot shows, the temperature modelling did not respond well. It was still decided to keep the hole run in the same figure, to illustrate the impact of the trip in and out.

In addition, the 9 5/8" casing was deformed several places resulting in that the clearance between the casing and drill string was less than modelled. This may have contributed to a higher actual ECD. Further it also turned out that drill pipe protectors were installed on the drill pipes. The manufacturer of drill pipe protectors claims that the ECD is only 0.03 SG, but the real actual impact is unknown. Overall, this justifies some of the discrepancies shown in *Figure 4.7.*

Due to all these complexities, this section is considered to be an outlier in the dataset.

5.3.2 Discussion - Loris-567_6in

Figure 4.8 show ECD-values crossing both pore- and fracture pressure through the 6-$inch$ section. Pore- and fracture pressure decreases due to a depleted reservoir zone. Simulations with actual parameters illustrated lower ECD-values compared the simulations with planning parameters. Actual ECD-values are higher than all the simulated ECD-values at all the different bit depths, giving only negative delta values in *Table 4.6*. For this 6-$inch$ section, average delta value is -0.037 SG with cuttings, while average delta value is -0.042 SG without cuttings. Maximum deviation value for delta with cuttings was -0.038 SG. The temperature plot is missing the actual annulus temperature because it was not available (N.A.) from the downhole tools used. Furthermore, temperature correction of simulated annulus temperature with actual parameters was not applicable due to the missing information. In other words, this means that bit depth vs temperature in *Figure 4.8* is not very relevant to look at, yet it is included to follow the structure of the thesis.

During drilling of this Loris-567_6in section, loss of return was encountered at 4099 $meters$. This explains why the actual ECD measured values stops at a bit depth of approximately 4070 $meters$, since the annular pressure sensor in the bottom hole assembly (BHA) is offset to the bit depth by typically around 30 $meters$. While recovering the well and establishing volume control, the string got stuck. Attempted to pull free utilizing the jar, which resulted in an increase in the loss rate. They also attempted to cure losses with LCM without success. String was cut with wireline, and wellbore was plugged and abandoned. In total, 11 days was spent on attempting to free BHA and securing the well. This is another example of why studies related to the topic of ECD and well control is important.

6. Uncertainties

The results obtained contain several uncertainties that will be mentioned and discussed in this chapter.

Generalized temperature gradient

A generalized temperature gradient of $\frac{3.5\ ℃}{100\ m}$ has been used to describe the expected formation temperature at different depths as per the well design basis. This presents a challenge, as the actual formation temperatures are likely different, and not homogenous throughout the well. Thus, either smaller or larger deviations in the bit depth vs temperature plots may occur, if one compares it with completely accurate temperature data, i.e., where a generalized temperature model is not used.

Steady-state hydraulic model

Steady-state hydraulic model implies that the simulations implemented, are based on a snapshot in time with predefined parameters for the current depth. Previous drilling parameters and operations are not considered for the calculations, i.e., generated cuttings and circulation rates. Furthermore, the "fluid-in" temperature is based on a chosen predefined value. Downhole in the well, the temperature increases, leading to larger deviations in the calculations of equivalent static density. Equivalent circulating density is a function of equivalent static density, and thus there will be deviations in the equivalent circulating density calculations.

There is a plan to implement a transient model that will take the operational sequence into account, but it has been decided that this model will be implemented at a later occasion. The reason for this is that a transient model is not necessary for most wells, in addition to the fact that a transient model is much more comprehensive to implement, compared to a steady-state model.

Assumptions made in the hydraulic model

The hydraulic model may contain assumptions that does not fit with the wells investigated in this thesis. DrillPlan builds on hydraulic motors from older Schlumberger software like Drilling Office X and Virtual Hydraulics, which both require many parameters. Developers and subject matter experts have pre-defined most of the parameters with a goal to simplify the use of DrillPlan. The parameters proposed are believed to best suit wells all around the world. The expression, one size does not fit all, can really appear here in some cases. There are continuous updates that adjust the assumptions and parameters. In addition, some parameters can be overridden in the system, if it turns out that one has historical experience with parameters that are more suitable. An example of an assumption is circulation time. Steady-state will only be reached after circulating with a constant pump rate for a certain time.

Heating and/or cooling of risers on the platform
The temperature profile does not consider heating and/or cooling as a result from either production or injection in other nearby wells in the risers on the platform.

Instability in the well
Parts of the well may collapse around the bottom hole assembly as result of; unstable formations, chemical reactions between drilling fluid and formation (e.g., swelling and breakout), faults and mechanical disturbances (often stabilizers and bit).

Error while entering data
Wrong choice of stabilizer, number of blades, thickness of blades, length of blades and profile of blades. Entered wrong diameter on components. It is also possible that the components may change before operation i.e., change of planned- versus dispatched equipment. This means that the bottom hole assemblies (BHAs) used for the simulations may not accurately reflect the BHAs used at the rig site.

Assumptions on drilling fluid parameters
DrillPlan assumes that the drilling fluid has the same properties through the drilling of the entire well, which is not the case in real life. As an example, the pressures exerted on the drilling fluid in deep wells will change the effective rheology of the fluid. During normal drilling operations it is not common to perform HTHP-rheology tests on the drilling fluid and the test are conducted under atmospheric conditions. Depending on the effect, this effect may be significant. The drilling fluid properties will alter continuously during drilling, due to cuttings particle suspension and possible contaminants downhole or at the surface.

Stabilizers and flow area
Flow area around the bottom hole assembly is largely affected by stabilizers. Stabilizers may have challenging three-dimensional shapes that can be difficult to model accurately, especially in a time-efficient manner. The effect of this is more significant in smaller hole sections such as 8.5-*inch* and 6-*inch*.

Incorrectly calibrated measuring equipment
While procedures are in place to ensure proper calibration, the measuring equipment on BHA for annular- pressure and temperature may have been incorrectly calibrated before operation.

Annular pressure sensor offset to bit depth
The annular pressure sensor in the bottom hole assembly (BHA) is offset to the bit depth by typically around 30 $meters$, but this varies depending on the BHA configuration. This offset has not been accounted for when comparing actual measured data versus simulated data using actual parameters.

Limited data set
All the three investigated wells are from the same location and of similar design, which results in limited data and similar simulations.

Inaccurate mapping of drilling parameters
During the data analysis, the drilling parameters obtained from operation had to be approximated and mapped to fit the available parameter range in the simulation results obtained from DrillPlan. Even if care was taken to map to the closest available parameter, deviations may have occurred.

Human error during simulation and processing of data sets
Results presented in this thesis may contain human errors from simulations and data processing.

7. Conclusion

The scope of this study was to investigate how accurate DrillPlan can model equivalent circulating density (ECD) for typical wells in the North Sea. The main findings show that the simplifications and prerequisites that DrillPlan implements, give results that vary with size and depth of drilled sections. Despite this, DrillPlan overall manages to simulate downhole conditions with sufficient accuracy.

DrillPlan managed to model expected ECD-values that was fairly similar to the actual ECD measured for the 13.5-*inch* section. The accuracy of modelled ECD-values was also quite high for the 12.25-*inch* section, although the deviations here were slightly larger than for the 13.5-*inch* section. One of the two 8.5-*inch* sections modeling showed that DrillPlan to some extent managed to simulate ECD-values that partly corresponded to the actual ECD-values, but with a lower accuracy than for the 13.5-*inch*- and 12.25-*inch* sections. When it comes to the other 8.5-*inch* section, a damaged casing, as well as the actual use of pipe protectors, may have contributed to the largest deviations found in this study between modeled ECD-values in DrillPlan and actual ECD-values measured. Results from this 8.5-*inch* section is therefore not considered representative unless the known deviations can be quantified. The 6-*inch* sections shows that DrillPlan is able to model ECD-values that can be compared to the actual ECD-values measured, but with a lower accuracy than the other representative 13.5-*inch*-, 12.25-*inch*- and 8.5-*inch* sections. Below *Table 7.1* shows an overview of the different average deviations between simulated ECD with- and without cuttings using actual parameters and actual measured ECD.

Table 7.1 Summary of average deviations found during validation of ECDs in the cloud-based well planning platform DrillPlan. The table listed below is sorted by the most accurate ECD modelling to least accurate ECD modelling, looking at values with- and without cuttings.

Name and section	**Average deviation with cuttings (SG)**	**Average deviation without cuttings (SG)**
Loris-234_13.5in	0.007	-0.012
Loris-234_12.25in	-0.006	-0.017
Loris-345_8.5in	-0.013	-0.020
Loris-345_6in	-0.020	-0.035
Loris-567_6in*	-0.037	-0.042
Loris-567_8.5in**	-0.098	-0.107

*Temperature not calibrated due to lack of downhole temperature data.

**Not considered representative due to additional uncertainties which is not quantified.

Based on the findings in this study, DrillPlan is fully capable of providing valid ECD calculations for well planning. For now, there is a need to calibrate the temperature profile of the sections, but this will be addressed in planned software upgrades. It is recommended to rerun simulations close to execution with measured rheology and actual BHAs to ensure the validity of the simulations.

7.1 Further work

DrillPlan is a cloud-based platform under continuous development, based on feature roadmaps, planned improvements and requests from clients and Schlumberger users. Work is ongoing to implement more advanced simulation engines on multiple areas. When the implementation is released, a new study should be conducted to validate how well the improvements work for the wells compared to this thesis.

As discussed in Chapter 6, *Uncertainties*, there are many uncertainties that affect the outcome of the comparison of simulated values against actual measurements. A separate study should be conducted to identify and quantify the impact of the uncertainties listed, for use in a comparison study.

Additionally, a more extensive comparison should be conducted on a greater variety of well designs, including vertical wells, horizontal wells, different drilling fluid systems (in this study, the same drilling fluid system was used in five out of six sections) and different temperature gradients.

8. References

[1] Oljedirektoratet, "Ressursrapport 2020," Stavanger. Accessed: May 05, 2022. [Online]. Available: https://www.npd.no/fakta/publikasjoner/rapporter/ressursrapporter/ressursrapport-2020/innledning-og-sammendrag/.

[2] B. S. Aadnoy and J. C. Russ, *Modern Well Design*, 2nd ed. Taylor & Francis Group, 2010.

[3] Statoil, "Rapport - Brønnhendelse Gullfaks C," 2010. Accessed: Apr. 22, 2022. [Online]. Available: https://www.equinor.com/news/archive/2010/11/05/05NovGullfaksCreport.

[4] E. Søbye, "Borekostnadene på sokkelen: Knask eller knep?," 2017. https://www.ssb.no/energi-og-industri/artikler-og-publikasjoner/borekostnadene-pa-sokkelen-knask-eller-knep (accessed May 03, 2022).

[5] Schlumberger, "DrillPlan Solution Improves Well Planning Efficiency by More Than 50%, Williston Basin." https://www.slb.com/resource-library/case-study/so/drillplan-willistonbasin-cs (accessed May 02, 2022).

[6] M.-I. SWACO, "Drilling Fluids Engineering Manual Version 2.2," 2009.

[7] B. Guo and G. Liu, "Equipment in Mud Circulating Systems," in *Applied Drilling Circulation Systems, Hydraulics, Calculations and Models*, 2011, pp. 3–18.

[8] R. F. Mitchell and S. Z. Miska, *Fundamentals of Drilling Engineering*, Volume 12. Society of Petroleum Engineers, 2010.

[9] American Petroleum Institute, "Rheology and Hydraulics of Oil-well Drilling Fluids (API Recommended Practice 13D Seventh Edition)," 2017.

[10] Schlumberger Oilfield Glossary, "Thixotropy." https://glossary.oilfield.slb.com/en/terms/t/thixotropy (accessed Mar. 11, 2022).

[11] Schlumberger Oilfield Glossary, "Marsh funnel." https://glossary.oilfield.slb.com/en/terms/m/marsh_funnel (accessed Feb. 07, 2022).

[12] Schlumberger, "Easily and Precisely Sample Water-, Oil-, or Synthetic-Based Drilling Fluid on Location." https://www.slb.com/drilling/drilling-fluids-and-well-cementing/drilling-fluids/drilling-fluids-simulation-software/rheoprofiler-automated-rheometer (accessed Feb. 08, 2022).

[13] "RP200 - Rheology and Density Test Procedure," 2020. https://web.microsoftstream.com/video/a912b8cc-9509-4443-9772-77ae8052ab03?referrer=https:%2F%2Fintouchsupport.com%2F (accessed Feb. 08, 2022).

[14] Cameron, "Rheoprofiler Z-015 Datasheet," 28-055-PD10-A-XC–011, 2020.

[15] K. P. Hoelscher, "Digitalization and Automation of the Oilfield (SPE Hydraulic Fracturing Technology Conference and Exhibition 4-6 February 2020)," 2020, pp. 1–10.

[16] Halliburton, "BaraLogix." https://www.halliburton.com/en/products/baralogix (accessed Mar. 15, 2022).

[17] Intelligent Mud Solutions, “About us.” https://www.imudsolutions.com/about-us (accessed Mar. 15, 2022).

[18] Intelligent Mud Solutions, “Our Tool Kit.” https://www.imudsolutions.com/our-tool-kit (accessed Mar. 15, 2022).

[19] Schlumberger Oilfield Glossary, “Herschel-Bulkley fluid.” https://glossary.oilfield.slb.com/en/terms/h/herschel-bulkley_fluid (accessed Feb. 08, 2022).

[20] H. J. Skadsem, A. Leulseged, and E. Cayeux, “Measurement of drilling fluid rheology and modeling of thixotropic behavior,” *Appl. Rheol.*, vol. 29, no. 1, pp. 1–11, 2019, doi: https://doi.org/10.1515/arh-2019-0001.

[21] R. Caenn, H. C. H. Darley, and G. R. Gray, *Composition and Properties of Drilling and Completion Fluids*, 6th ed. Elsevier Science & Technology, 2011.

[22] Schlumberger Oilfield Glossary, “Mud density.” https://glossary.oilfield.slb.com/en/terms/m/mud_density (accessed Feb. 10, 2022).

[23] S. Naganawa and K. Okatsu, “Fluctuation of Equivalent Circulating Density in Extended Reach Drilling with Repeated Formation and Erosion of Cuttings Bed,” *IADC/SPE Asia Pacific Drill. Technol. Conf. Exhib. Jakarta, Indones.*, 2008, doi: https://doi.org/10.2118/115149-MS.

[24] M. Zamora, P. N. Broussard, and M. P. Stephens, “The Top 10 Mud-Related Concerns in Deepwater Drilling Operations,” *SPE Int. Pet. Conf. Exhib. Mex. IPCEM*, 2000, doi: https://doi.org/10.2118/59019-MS.

[25] M. Zamora and S. Roy, “The Top 10 Reasons to Rethink Hydraulics and Rheology,” *Proc. IADC/SPE Asia Pacific Drill. Technol. Conf. APDT*, 2000, doi: https://doi.org/10.2118/62731-MS.

[26] R. Rommetveit and K. S. Bjorkevoll, “Temperature and Pressure Effects on Drilling Fluid Rheology and ECD in Very Deep Wells,” *SPE/IADC Middle East Drill. Technol. Conf.*, 1997, doi: https://doi.org/10.2118/39282-MS.

[27] V. C. Kelessidis, R. Maglione, C. Tsamantaki, and Y. Aspirtakis, “Optimal determination of rheological parameters for Herschel–Bulkley drilling fluids and impact on pressure drop, velocity profiles and penetration rates during drilling,” *Pet. Sci. Eng.*, vol. 53, no. 3–4, pp. 203–224, 2006, doi: https://doi.org/10.1016/j.petrol.2006.06.004.

[28] K. Founargiotakis, V. C. Kelessidis, and R. Maglione, “Laminar, transitional and turbulent flow of Herschel-Bulkley fluids in concentric annulus,” *Can. J. Chem. Eng.*, vol. 86, no. 4, pp. 676–683, 2008, doi: https://doi.org/10.1002/cjce.20074.

[29] V. Dokhani, Y. Ma, Z. Li, T. Geng, and M. Yu, “Effects of drill string eccentricity on frictional pressure losses in annuli,” *J. Pet. Sci. Eng.*, vol. 187, no. March 2019, 2019, doi: https://doi.org/10.1016/j.petrol.2019.106853.

[30] M. Haciislamoglu and J. Langlinais, “Non-Newtonian Flow in Eccentric Annuli,” *J. Energy Resour. Technol. Trans. ASME*, vol. 112, no. 3, pp. 163–169, 1990, doi: https://doi.org/10.1115/1.2905753.

[31] E. Cayeux, “Mathematical Modelling of the Drilling Process for Real-time

Applications in Drilling Simulation , Interpretation and Assistance," University of Stavanger, 2019.

[32] M. Haciislamoglu and U. Cartalos, "Practical Pressure Loss Predictions in Realistic Annular Geometries," *SPE 28304*, pp. 113–126, 1994, doi: https://doi.org/10.2118/28304-MS.

[33] A. Saasen, "Annular Frictional Pressure Losses During Drilling—Predicting the Effect of Drillstring Rotation," *J. Energy Resour. Technol.*, vol. 136, no. 3, pp. 1–5, 2014, doi: https://doi.org/10.1115/1.4026205.

[34] Schlumberger, "Welcome to DrillPlan - Validation - Hydraulic Analysis." https://guru.delfi.slb.com/content/1003/help/52B31D93-D782-436A-95D9-C49C52563CA1 (accessed May 13, 2022).